minerals

MDPI

Article

Genesis of Graphite Mineralization in the Kambale Graphite Deposit, Wa-Lawra Belt, Ghana: Evidence from Petrography, Geochemistry, and Stable Carbon Isotopes

Emmanuel Daanoba Sunkari [1,2,3,*], Etornam Bani Fiadonu [4], Mehmet Ali Gücer [5], Yılmaz Demir [6], Joseph Ndago Amoldago [1,2], Arnold Nuru Gan [4], Bismark Mensah [4], Samuel Edem Kodzo Tetteh [7], Salaam Jansbaka Adams [8] and Abdurrahman Lermi [9]

1 Mining Engineering, Department of Integrated and Advanced Technology, School of Engineering and Sciences, Sir Padampat Singhania University, Udaipur 313 601, Rajasthan State, India; amoldagojosph122@gmail.com
2 Centre of Excellence in Environmental Science and Sustainability, Directorate of Environment and Ecology, Sir Padampat Singhania University, Udaipur 313 601, Rajasthan State, India
3 Department of Chemical Sciences, Faculty of Science, University of Johannesburg, Auckland Park 2006, Johannesburg P.O. Box 524, South Africa
4 Department of Geological Engineering, Faculty of Geosciences and Environmental Studies, University of Mines and Technology, Tarkwa P.O. Box 237, Ghana; ebfiadonu@umat.edu.gh (E.B.F.); nuruganarnold@gmail.com (A.N.G.); bismarkmensah183@gmail.com (B.M.)
5 Department of Geological Engineering, Gümüşhane University, 29000 Gümüşhane, Türkiye; maligucer@gmail.com
6 Department of Geological Engineering, Faculty of Engineering and Architecture, Recep Tayyip Erdoğan University, Main Campus, 53100 Rize, Türkiye; yilmaz.demir@erdogan.edu.tr
7 Onyx Gold Corp., 375 Water Street, Suite 405, Vancouver, BC V6B 5C6, Canada; tsekman28@gmail.com
8 Department of Geography and Earth Sciences, School of Natural and Environmental Sciences, University of Environment and Sustainable Development, Private Mail Bag, Somanya, Eastern Region, Ghana; sajansbaka@uesd.edu.gh
9 Department of Geological Engineering, Faculty of Engineering, Niğde Ömer Halisdemir University, Main Campus, 51240 Niğde, Türkiye; alermi@ohu.edu.tr
* Correspondence: emmanueldaanobasunkari@gmail.com

Abstract

Graphite is a critical raw material for emerging energy technologies, yet the origin of many Paleoproterozoic graphite deposits remains poorly constrained. This study presents the first integrated investigation of graphite mineralization at the Kambale Graphite Deposit in the Wa–Lawra Belt of northwestern Ghana, combining field observations, petrographic, SEM-BSE/EDX, whole-rock geochemistry, total carbon content (%C), and stable carbon isotope ($\delta^{13}C$) analyses. Graphite occurs predominantly as fine crystalline flakes associated with quartz and muscovite and aligned parallel to the schistosity, consistent with syn-metamorphic recrystallization and deformation-assisted grain coarsening. Accessory pyrrhotite is closely associated with graphite within graphite schists. Graphite mineralization occurs within graphitic metasedimentary units, whereas the associated gneisses and metagranodiorite are interpreted as granitoid-derived meta-igneous rocks. Trace-element and REE characteristics, including LREE enrichment and negative Nb-Ta-Ti anomalies, indicate that the gneisses and metagranodiorite were derived from evolved continental crust and originated from granitic to granodioritic protoliths in a continental arc setting. The graphite schists contain 0.58–17.29%C, while their stable carbon isotope compositions ($\delta^{13}C$ = −31.83‰ to −24.33‰ VPDB) support an organic-derived carbon source. The mineral assemblages are consistent with lower amphibolite-facies metamorphism, which facilitated the graphitization and recrystallization of sedimentary organic carbon. The deposit formed through deposition of carbonaceous sediments followed by Eburnean

Check for updates

Academic Editors: Argyrios Papadopoulos, Panagiotis Voudouris and Constantinos G. Mavrogonatos

Received: 27 August 2026
Revised: 20 September 2026
Accepted: 20 September 2026
Published: 15 October 2026

Copyright: © 2026 by the authors. Licensee MDPI, Basel, Switzerland. This article is an open access article distributed under the terms and conditions of the Creative Commons Attribution (CC BY) license.

metamorphism and deformation, providing a framework for graphite exploration in the West African Craton.

Keywords: graphitization; metamorphogenic graphite; carbon isotopes; amphibolite-facies metamorphism; Wa-Lawra Belt

1. Introduction

Graphite has emerged as a critical mineral due to its essential role in modern energy systems and high-technology applications [1,2]. It is the dominant anode material in lithium-ion batteries and is therefore central to the global expansion of electric vehicles and renewable energy storage technologies [1,3]. Beyond energy storage, graphite is widely used in nuclear reactors, refractories, lubricants, and advanced electronic materials because of its high thermal conductivity, chemical inertness, and lubricating properties [4,5]. Increasing demand, coupled with supply-chain concentration and geopolitical risks, has intensified global efforts to identify new sources of high-quality crystalline graphite [2,6].

Most economically viable graphite deposits form through metamorphism of carbon-rich sedimentary protoliths [4,7]. During regional metamorphism, organic carbon undergoes progressive structural reorganization, resulting in crystalline graphite [4,8]. The degree of graphitization is strongly controlled by metamorphic temperature and pressure [7,9]. Poorly ordered graphite typically forms under greenschist-facies conditions, whereas well-ordered and coarse flake graphite develops under amphibolite- to granulite-facies metamorphism [8,10]. Fully ordered graphite generally forms at temperatures above approximately 500 °C [2,7], making metamorphic grade a primary control on graphite quality and economic potential.

Geochemical approaches provide robust constraints on the origin and evolution of graphite-bearing rocks [11,12]. High-field-strength elements (HFSE) and rare earth elements (REE) are particularly valuable because they remain relatively immobile during weathering, sedimentary recycling, and metamorphism [11,12]. Their distributions preserve information on sediment provenance and tectonic setting [12,13]. Stable carbon isotope compositions ($\delta^{13}C$) provide an additional constraint on carbon sources. Organic carbon generally exhibits relatively light $\delta^{13}C$ values, commonly around −22‰ to −27‰ [14,15], although values outside this range may occur depending on the nature of the organic precursor, depositional environment, and subsequent diagenetic or metamorphic processes [4,8]. In contrast, inorganic carbon derived from mantle fluids or carbonate decarbonation generally exhibits heavier $\delta^{13}C$ values, typically ranging from approximately −5‰ to +5‰ [4,8]. Recent studies emphasize the importance of integrating whole-rock geochemistry and carbon isotope data to distinguish sedimentary–metamorphic graphite from graphite influenced by CO_2-rich fluids [10,13].

The Paleoproterozoic Birimian terranes of West Africa are well known for their gold endowment [16–18]. However, recent investigations have highlighted their potential for graphite mineralization [19,20]. In north-western Ghana, the Wa-Lawra Belt has emerged as a promising graphite-bearing terrane [19,20]. The belt is dominated by metasedimentary and metavolcanic rocks and is characterized by a distinct north–south structural trend [19]. It has experienced medium-to high-grade regional metamorphism, creating favorable conditions for graphite crystallization [19,20].

The Kambale Graphite Deposit is located within the Wa–Lawra Belt of northwestern Ghana and is hosted mainly by graphite schists and quartz–mica schists [19,20]. Previous studies estimated peak metamorphic conditions in the area at approximately 600–750 °C

and 5.0–8.0 kbar, corresponding broadly to amphibolite-facies conditions [19,20]. Despite increasing exploration interest and reported resource potential, the metamorphic evolution of the host rocks and the source of carbon at Kambale remain insufficiently constrained. In particular, it is unclear whether the graphite formed entirely through metamorphism of organic-rich sediments or whether additional carbon was introduced or modified by deep-seated CO_2-rich fluids.

Previous work by [19] provided a preliminary assessment of the geological and structural controls of graphite mineralization at Kambale based on field investigations, trench mapping, RAB drill-hole logging, and petrographic observations, while [20] presented petrographic and SEM-BSE/EDX observations of the lithological and mineralogical characteristics of the graphite ore at the VI International Turkic World Congress on Science and Engineering (TURK-COSE 2024). The present study incorporates selected SEM-BSE/EDX observations from [20], which are re-evaluated in conjunction with an entirely new petrographic dataset and expanded datasets comprising whole-rock major-, trace-, and rare earth element geochemistry, total carbon content (%C), and stable carbon isotope ($\delta^{13}C$) analyses. Thus, although some SEM-BSE/EDX observations overlap with [20], the petrographic observations presented here are newly acquired, and the present study extends the earlier work by integrating these complementary datasets to constrain the carbon source, protolith characteristics, depositional conditions, metamorphic evolution, and processes responsible for graphite mineralization, and to develop a comprehensive genetic model for the Kambale Graphite Deposit.

Combining mineralogical and microstructural observations with whole-rock geochemistry and stable carbon isotope data provides a more comprehensive basis for evaluating graphite genesis than individual analytical approaches [4,10,13]. Stable carbon isotopes provide important constraints on the origin of carbonaceous material and can help distinguish organic sedimentary carbon from carbon associated with inorganic or CO_2-rich sources [4,10]. Such deposit-scale integrated investigations remain limited in Paleoproterozoic terranes, including the Wa–Lawra Belt. The present study therefore contributes new geological and geochemical constraints on the formation of metamorphogenic flake graphite at Kambale and provides a basis for evaluating its development within the Eburnean tectono-metamorphic evolution of the belt. A better understanding of the geological processes controlling natural graphite mineralization is also relevant to the responsible development of graphite resources, given the importance of graphite as a critical raw material for energy-storage and low-carbon technologies [1,5].

Therefore, this study seeks to: (i) characterize the petrographic and mineralogical characteristics of the graphite-bearing rocks and their relationship to graphite mineralization; (ii) determine the provenance, depositional environment, and tectonic setting of the protoliths using whole-rock major-, trace-element, and rare earth element geochemistry; (iii) constrain the source of carbon using stable carbon isotope ($\delta^{13}C$) analysis; and (iv) develop an integrated genetic model for graphite mineralization within the Eburnean tectono-metamorphic evolution of the Paleoproterozoic Wa–Lawra Belt.

2. Geological Setting

The Kambale Graphite Deposit is located in northwestern Ghana within the Wa-Lawra Belt, a Paleoproterozoic volcano-sedimentary belt of the Birimian Supergroup in the West African Craton (Figure 1). The Birimian terrane comprises metavolcanic, metasedimentary, volcaniclastic, and granitoid rocks that were deformed and metamorphosed during the Eburnean Orogeny (ca. 2.2–2.1 Ga) [19–23]. Regional deformation and metamorphism associated with the Eburnean event produced the dominant structural and metamorphic framework of the belt [24,25].

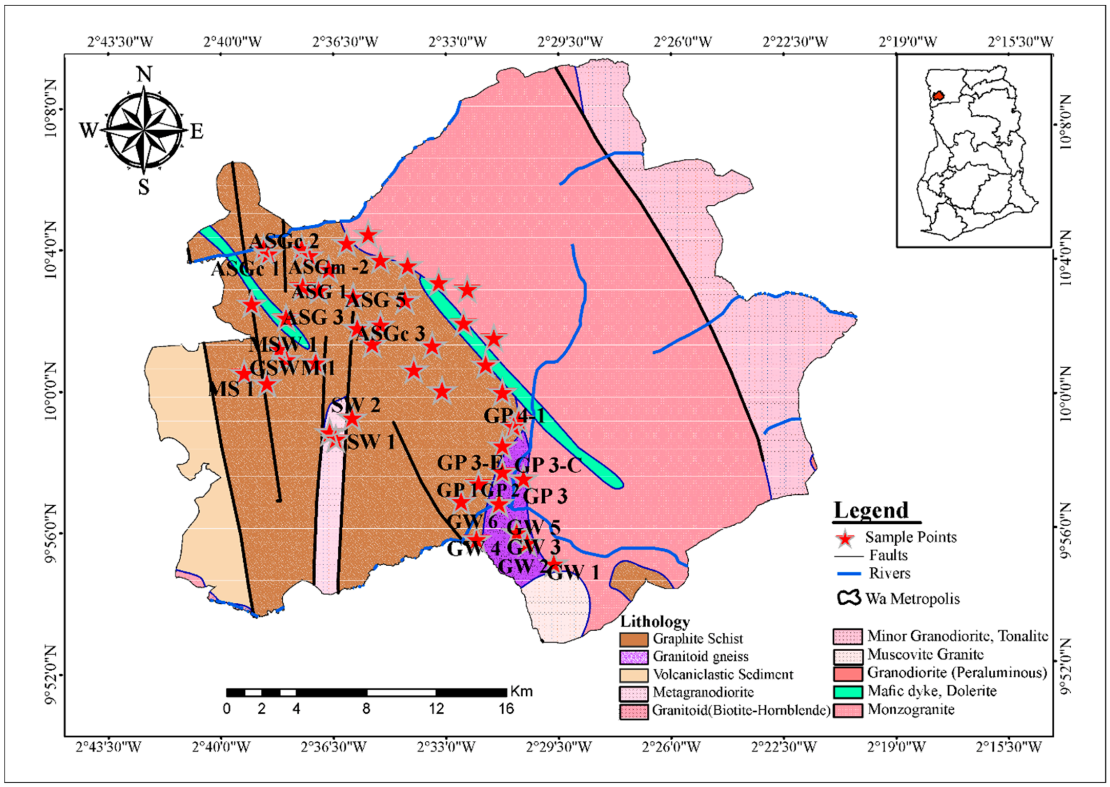


Figure 1. Geological map of the Kambale Graphite Deposit, Wa-Lawra Belt, northwestern Ghana, illustrating the spatial distribution of graphite-bearing lithologies, granitoids, mafic dykes, faults, drainage systems, and sampling locations. The inset shows the detailed sampling area and the geographic location of the study area within Ghana. The graphitic mineralization occurs mainly within schistose and gneissic units associated with granitoid intrusions and is structurally controlled.

The Wa-Lawra Belt forms the southern continuation of the Boromo Belt of Burkina Faso and is bounded by granitoid domains and adjacent Birimian belts [21]. The belt is structurally controlled by major faults and shear zones, including the Jirapa Fault system, which segment the belt into distinct lithostructural domains [22]. The dominant structural grain trends NNE-SSW to NE-SW and reflects the regional Eburnean deformation pattern [22,25].

Lithologically, the belt consists of metavolcanic, metasedimentary, and volcaniclastic rocks intruded by granitoids (Figure 1) and locally metamorphosed from greenschist- to amphibolite-facies conditions [19,21,22,26]. The Kambale deposit is hosted predominantly by graphitic schist, mica schist, and quartz–mica schist, with minor phyllite and pegmatitic intrusions [19]. Graphite mineralization occurs within laterally continuous stratabound horizons hosted by the graphitic metasedimentary sequence.

The area records multiple phases of deformation. Early deformation resulted in the development of penetrative foliation and steeply dipping shear zones, whereas later deformation produced folding, crenulation cleavage, and quartz-filled veins [22,27]. These structures strongly influence the geometry and continuity of the graphite-bearing horizons.

3. Materials and Methods

3.1. Field Studies and Sample Collection

Field investigations were conducted at the Kambale Graphite Deposit in October 2024 to document the regional and local geological setting, lithological relationships, structural features, and occurrence of graphite mineralization. A total of fifty (50) representative samples of graphite-bearing rocks, including graphite schists and gneisses, and associated

lithologies, including metagranodiorite, were collected from different locations across the study area. Particular attention was given to graphite-bearing horizons and their relationships with the surrounding metamorphic rocks and felsic intrusive bodies. Graphite schist was generally highly weathered at most outcrops; consequently, only the freshest and least-altered material was selected for laboratory analysis. The collected samples were selected to capture the observed lithological, mineralogical, and textural variations within the study area and were subsequently used for petrographic, scanning electron microscopy with backscattered electron imaging and energy-dispersive X-ray spectroscopy (SEM-BSE/EDX), whole-rock geochemical, and total carbon and stable carbon isotope analyses.

3.2. Petrographic Analysis

A total of 20 representative samples were selected for petrographic analysis, including the graphite schist sample CK0004-1, which was examined in detail to characterize the textural relationships among graphite, quartz, muscovite, and associated minerals. Thin sections were prepared at the Department of Geological Engineering, Gümüşhane University, Türkiye. Mineralogical and petrographic examinations were performed using a Leica DM750 P polarizing microscope (Leica Microsystems, Heerbrugg, Switzerland), and photomicrographs were acquired with an attached Leica DFC450 digital camera (Leica Microsystems, Heerbrugg, Switzerland) to characterize the mineral assemblages, textures, and mineral relationships in the variably metamorphosed rocks. The study focused on identifying primary and secondary minerals, documenting their textural characteristics, and classifying the rock types. Mineral abbreviations used in the photomicrographs follow Whitney and Evans [28].

3.3. SEM-BSE/EDX Analysis

The microstructural characteristics and mineralogical features of graphite-bearing rocks were investigated using scanning electron microscopy with backscattered electron imaging and energy-dispersive X-ray spectroscopy (SEM-BSE/EDX, Carl Zeiss Microscopy GmbH, Jena, Germany) at the Environmental Monitoring Laboratory, University of Mines and Technology, Ghana. A total of 10 representative samples were selected for SEM-BSE/EDX analysis. The analyses enabled detailed examination of graphite morphology, including flake size, distribution, textural relationships, and deformation features, as well as qualitative chemical characterization of graphite and associated mineral phases.

3.4. Whole-Rock Geochemical Analysis

A total of 15 representative rock samples were selected for whole-rock geochemical analysis at Bureau Veritas Commodities Canada Ltd., Vancouver. The analyzed suite comprised one metagranodiorite sample (SW1), two graphite schist samples (MSW-1 and ASG-2M), and twelve gneiss samples. Prior to analysis, the samples were washed with 99.5% ethanol to minimize contamination and oven-dried at low temperature to remove residual moisture. The dried samples were crushed to approximately 70% passing <2 mm and subsequently pulverized to 85% passing <76 μm. Major element compositions were determined using the LF300 analytical procedure, involving $LiBO_2/Li_2B_4O_7$ fusion of 0.2 g of powdered sample followed by Inductively Coupled Plasma Emission Spectrometry (ICP-ES). Trace elements and rare earth elements (REEs) were analyzed using the MA250 analytical procedure, involving four-acid digestion of 0.25 g of powdered sample followed by ultra-trace Inductively Coupled Plasma Mass Spectrometry (ICP-MS; Thermo Fisher Scientific, Bremen, Germany). The quality of the ICP-MS data was assessed by Bureau Veritas using certified reference materials, analytical blanks, preparation blanks, and repeat analyses. The quality-control report documents the use of OREAS45H, OREAS501D, SO-19,

OREAS30A, and GGC-09 reference materials for the analytical procedures (details in Supplementary Table S1). Repeat analyses were performed to evaluate analytical reproducibility; for example, replicate analysis of sample SW1 yielded closely comparable concentrations for the analyzed elements, indicating good analytical precision. The analytical results were subjected to laboratory quality-control and data-validation procedures prior to issuance of the final certificate. The whole-rock geochemical data were used to characterize the bulk chemical composition of the studied lithologies and to assess sediment provenance and depositional conditions. Only one metagranodiorite sample (SW1) was analyzed; therefore, the geochemical characteristics reported for the metagranodiorite are considered representative of the analyzed sample and should not be regarded as representative of the entire metagranodiorite unit.

3.5. Total Carbon (%C) and Stable Carbon Isotope Analysis

Seventeen representative graphite schist samples from the ore zone were selected for total carbon and stable carbon isotope ($\delta^{13}C$) analyses at the Stable Isotope Laboratory, Cornell University, USA. Total carbon content was determined by elemental analysis and reported as carbon percentage (%C) by weight. Carbon isotope compositions were measured using a Thermo Delta V isotope-ratio mass spectrometer (IRMS; Thermo Fisher Scientific, Bremen, Germany) interfaced with an NC2500 elemental analyzer (Carlo Erba Instruments, Milan, Italy) and are reported in delta notation ($\delta^{13}C$) relative to the Vienna Pee Dee Belemnite (VPDB) standard. The $\delta^{13}C$ values are reported to two decimal places based on the laboratory analytical precision, with an analytical uncertainty of approximately $\pm 0.23‰$ (1σ). Quality assurance and quality control (QA/QC) procedures followed standard protocols used by the Cornell Isotope Laboratory. In-house reference materials were routinely calibrated against internationally recognized standards provided by the International Atomic Energy Agency (IAEA), ensuring traceability and comparability of isotope measurements. Instrument precision and long-term stability were monitored throughout the analytical sequence. An in-house standard (GNPS) was analyzed after every ten samples to assess instrument accuracy and precision. For the analytical run associated with this dataset, the long-term standard deviation (1σ) of the GNPS in-house standard was 0.23‰ for $\delta^{13}C$. Linearity effects were assessed using a methionine standard measured across a wide range of peak amplitudes; for $\delta^{13}C$, measurements across 5–370 V produced a linearity error of 0.10‰. In addition, all $\delta^{13}C$ values were validated using two USGS reference materials (USGS 40 and USGS 41a) to confirm accuracy across internationally calibrated scales (details in Supplementary Table S2). The isotopic compositions were ultimately expressed as $\delta^{13}C$ relative to the Vienna Pee Dee Belemnite (V-PDB) standard. The resulting total carbon and $\delta^{13}C$ data were used to evaluate the carbon source of the graphite-bearing rocks and to distinguish between predominantly organic and inorganic carbon sources.

4. Results

4.1. Field Relations and Petrography

4.1.1. Metagranodiorite

The metagranodiorite occurs as a dark-grey to whitish-grey, foliated unit with transitional characteristics between granitic gneiss and schist. It is cross-cut by discordant quartz veins up to 15–20 cm thick, and the foliation is moderately to steeply dipping (194°/66°) (Figure 2a,b).



Figure 2. Field exposure of the various graphite-bearing rocks and associated lithologies: (**a**,**b**) dark grey to whitish-grey, medium- to fine-grained metagranodiorite, (**c**,**d**) dark grey and fine-grained gneiss, (**e**–**h**) dark grey, fine-grained graphite schist showing moderate to intense weathering, and (**i**) graphitic schist intervals intersected from 18.6 m to 21.3 m and from 29.3 m to 36.1 m in a diamond drill hole (https://www.castleminerals.com/kambale: accessed on 19 September 2026).

Petrographically, the metagranodiorite is composed mainly of quartz, plagioclase, and hornblende, with minor K-feldspar (Figure 3a–d). Coarse primary quartz and plagio-

clase grains exhibit fracturing and embayed boundaries, while quartz displays prominent undulose extinction and recrystallization (Figure 3b). Fine-grained recrystallized quartz and hornblende define a weak foliation (Figure 3c). Hornblende occurs predominantly as subhedral to anhedral prismatic crystals with a weak preferred orientation, producing a nematoblastic to nematogranoblastic texture (Figure 3c). Potassium feldspar locally displays a perthitic texture and is associated with muscovite, quartz, and plagioclase (Figure 3d). The mineral assemblage and preservation of relict igneous textures are consistent with a granitoid protolith.

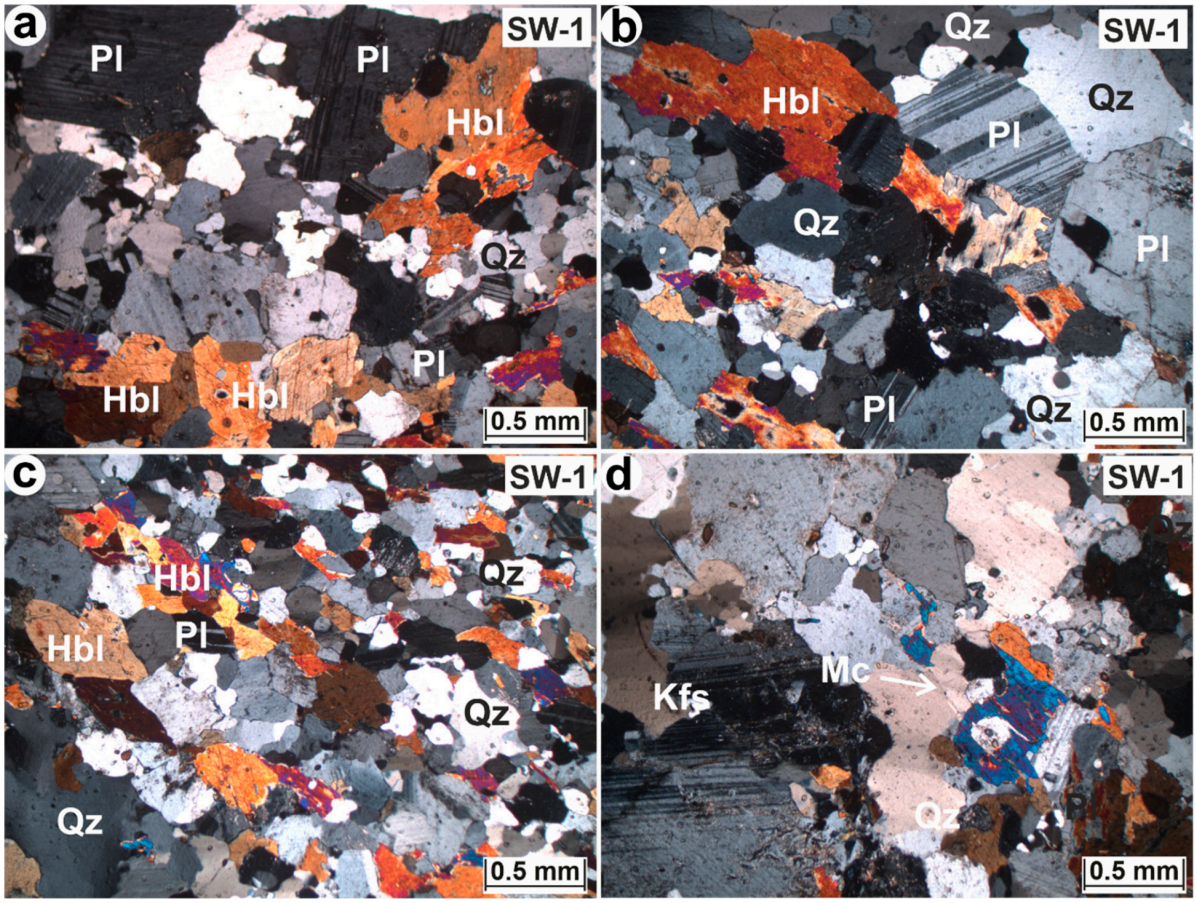


Figure 3. Photomicrographs of the metagranodiorite sample (SW-1) under crossed-polarized light showing the principal mineral assemblage and deformation features: (**a**) coarse-grained plagioclase (Pl), quartz (Qz), and hornblende (Hbl) defining the primary mineral assemblage, (**b**) hornblende associated with quartz and plagioclase, with quartz displaying undulose extinction and evidence of recrystallization, (**c**) fine-grained recrystallized quartz and hornblende forming a weak foliation, indicating metamorphic overprinting of the original igneous texture, and (**d**) potassium feldspar (Kfs) exhibiting perthitic texture and associated muscovite (Mc), together with quartz and plagioclase, reflecting deformation and alteration of the granitoid protolith. Abbreviations: Qz = quartz, Pl = plagioclase, Hbl = hornblende, Kfs = K-feldspar, Mc = muscovite.

4.1.2. Gneiss

The gneiss occurs as a dark-grey, fine-grained rock characterized by well-developed foliation and local compositional banding defined by the preferred alignment of biotite and muscovite (Figure 2c,d). Granitic intercalations of variable grain size are present within the gneiss and represent multiple intrusive episodes subsequently affected by deformation and metamorphism. Quartz and feldspar constitute the principal framework minerals and commonly display strain-related features such as recrystallization and undulose extinction. Locally, foliation wraps around feldspar porphyroclasts, indicating ductile deformation.

The gneiss is composed predominantly of quartz, plagioclase, K-feldspar, biotite, and epidote (Figure 4a–d). Coarse primary feldspar and quartz grains are preserved, while abundant fine-grained recrystallized quartz, biotite, and epidote record metamorphic overprinting. Biotite occurs as subhedral greenish-brown crystals, whereas epidote is commonly present as subhedral to anhedral grains, frequently enclosed within plagioclase (Figure 4a–d).

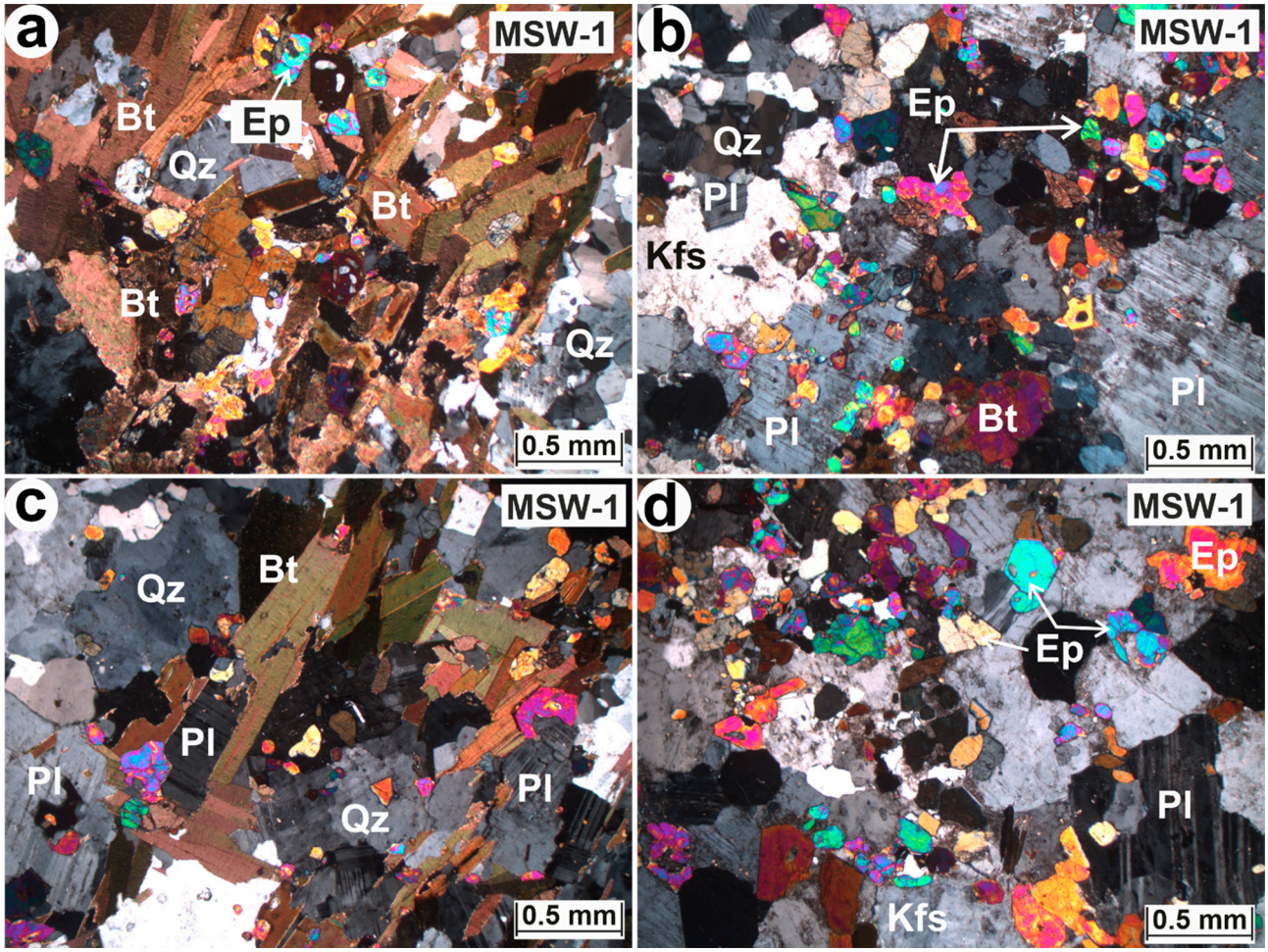


Figure 4. Photomicrographs of the gneiss sample (MSW-1) under crossed-polarized light showing the mineral assemblage and metamorphic textures: (**a**) biotite (Bt)-rich domain associated with quartz (Qz) and epidote (Ep), illustrating the micaceous character of the rock, (**b**) plagioclase (Pl) and quartz (Qz) with abundant epidote (Ep) occurring as subhedral to anhedral grains, indicating metamorphic recrystallization and alteration, (**c**) coarse biotite crystals intergrown with quartz and plagioclase, preserving relic igneous textures within the metamorphosed rock, and (**d**) epidote-rich assemblage associated with plagioclase and possible K-feldspar (Kfs), reflecting metamorphic overprinting and fluid-assisted alteration. Abbreviations: Qz = quartz, Pl = plagioclase, Bt = biotite, Ep = epidote, Kfs = K-feldspar.

4.1.3. Graphite Schist

The graphite schist occurs as dark grey to black, fine- to medium-grained lithologies characterized by well-developed schistosity and compositional banding defined by alternating graphite-rich and quartz–feldspar-rich layers (Figure 2a–h). The banding is commonly folded and locally disrupted by quartz–feldspar-rich veins and leucocratic segregations that occur parallel to or crosscut the foliation, reflecting multiple phases of deformation and intrusive activity (Figure 2a–c,g,h). Graphite-rich horizons are closely associated with the regional metamorphic fabric and commonly weather preferentially along foliation

planes. Diamond drilling confirmed the continuity of graphite mineralization at depth, with graphitic schist intersected between 18.6–21.3 m and 29.3–36.1 m (Figure 2i).

The rock is composed predominantly of quartz, muscovite, and graphite, with minor altered feldspar and secondary sericite, clay, and iron oxides (Figure 5a–d). Quartz, muscovite, and graphite define a pronounced schistosity and impart a predominantly lepidoblastic texture, while localized quartz and muscovite porphyroblasts produce porphyroblastic textures (Figure 5a–d). Muscovite commonly occurs as coarse, deformed, and fragmented flakes, whereas graphite occurs predominantly as fine-grained flakes, locally forming slightly coarser aggregates, aligned parallel to the foliation together with quartz and muscovite.

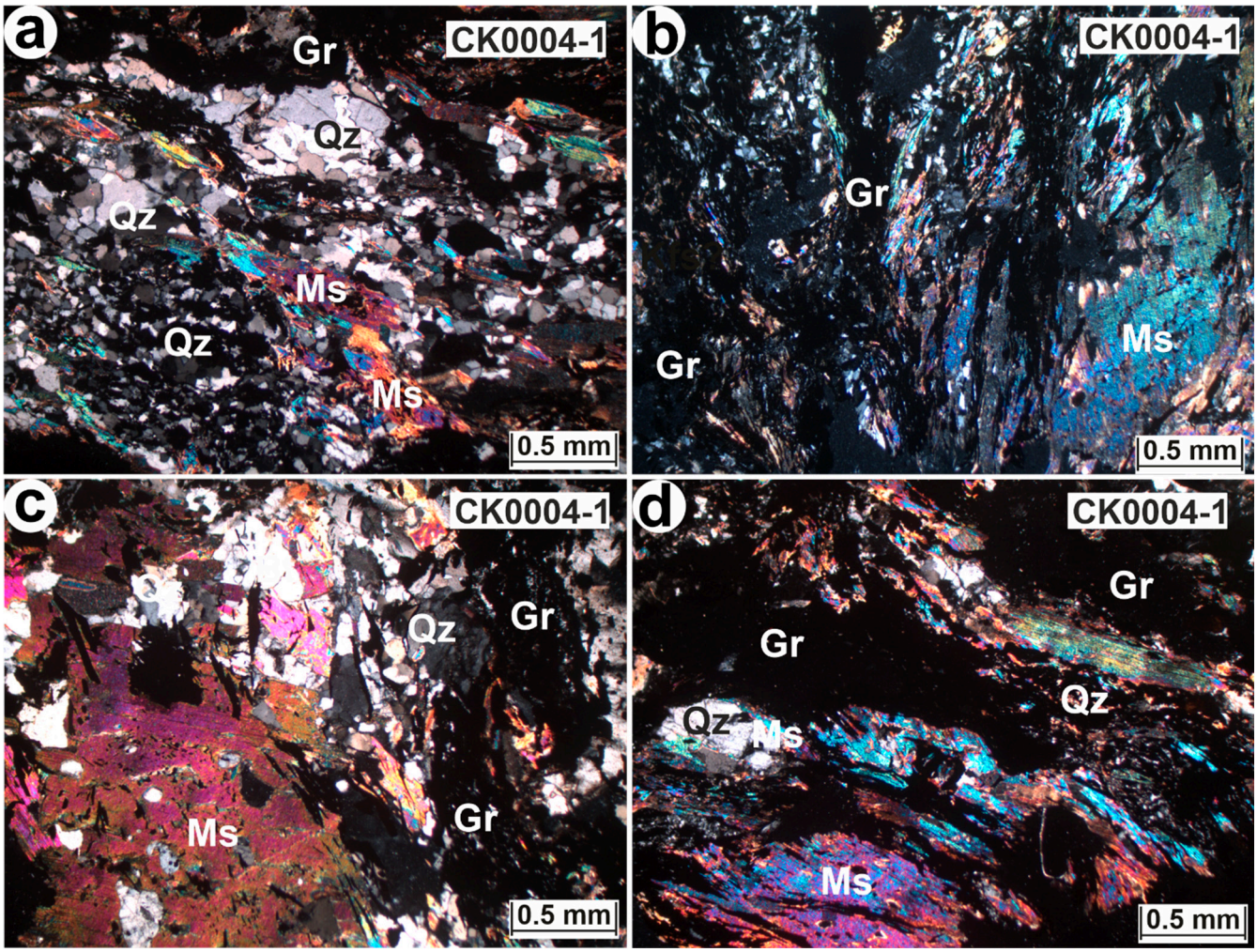


Figure 5. Photomicrographs of the graphite schist sample (CK0004-1) under crossed-polarized light showing the mineral assemblage and deformation fabrics: (**a**) well-developed schistosity defined by the alignment of graphite (Gr), muscovite (Ms), and quartz (Qz), producing a characteristic lepidoblastic texture, (**b**) graphite-rich bands interlayered with muscovite-rich domains, illustrating the strong preferred orientation of graphite flakes parallel to the foliation, (**c**) coarse muscovite associated with quartz and graphite, displaying localized porphyroblastic texture within the foliated matrix, and (**d**) alternating graphite- and quartz–muscovite-rich layers defining the compositional banding and schistosity of the rock. Abbreviations: Gr = graphite, Qz = quartz, Ms = muscovite.

4.2. SEM-BSE and EDX Characteristics

SEM-BSE imaging and EDX analyses provide high-resolution information on the microstructural characteristics and mineralogical relationships of the graphite-bearing rocks from the Kambale Graphite Deposit. In BSE images, graphite appears as dark-grey to black

flakes and aggregates, quartz and muscovite display intermediate grey tones, and pyrrhotite occurs as bright phases because of its higher average atomic number (Figure 6a–d).

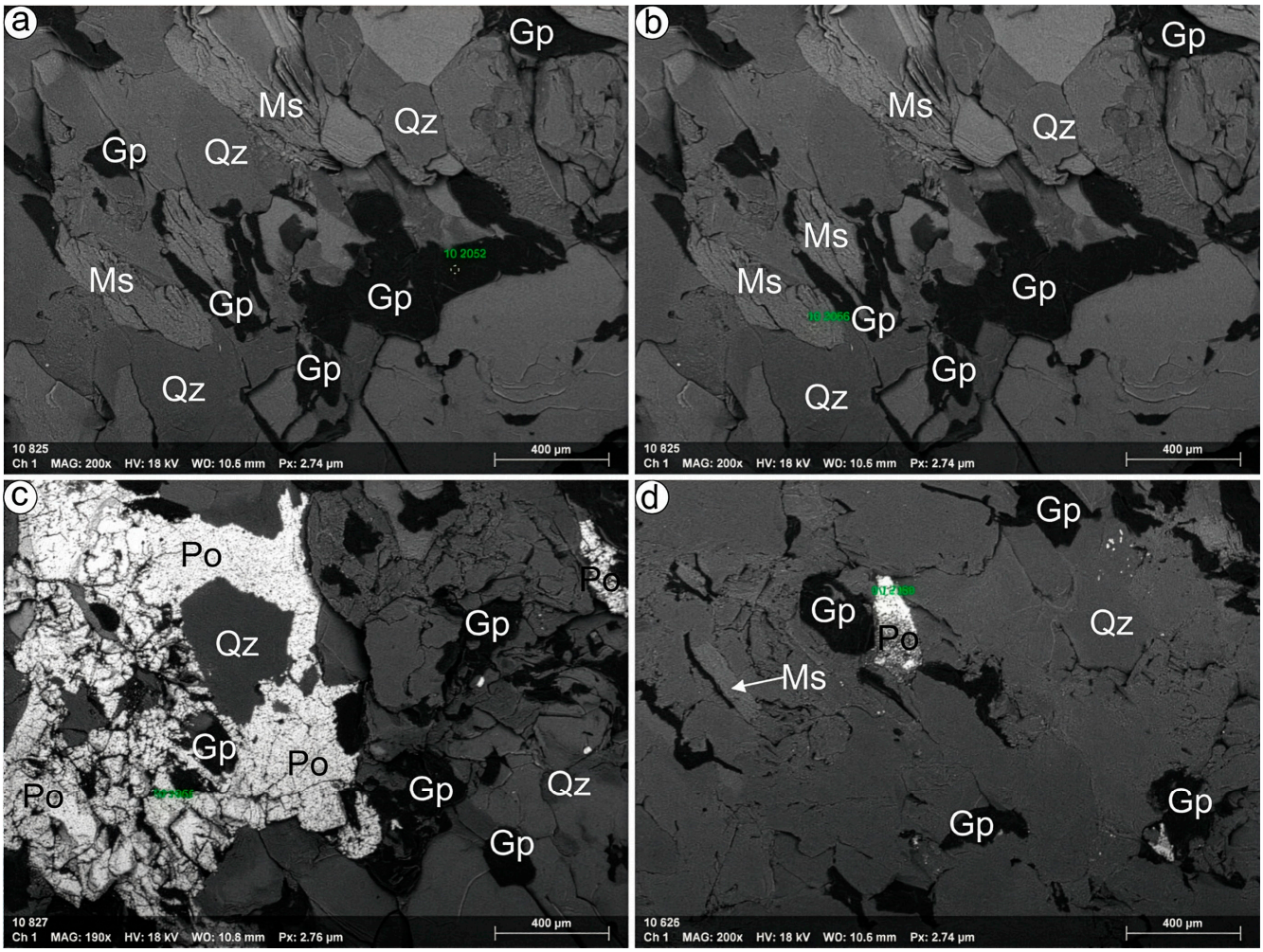


Figure 6. SEM-BSE images of graphite schist (CK0004-1) from the Kambale Graphite Deposit, Wa-Lawra Belt, Ghana: (**a**) intergrowth of graphite (Gp), quartz (Qz), and muscovite (Ms) showing graphite flakes distributed within a quartz–mica matrix, (**b**) graphite concentrated along muscovite-defined foliation planes, (**c**) bright pyrrhotite (Po) associated with graphite and quartz, indicating sulfide mineralization within the graphitic schist, and (**d**) disseminated pyrrhotite enclosed within a quartz–graphite–muscovite assemblage.

Graphite occurs as anhedral to subhedral flakes intergrown with quartz and muscovite and is commonly aligned parallel to the foliation defined by muscovite (Figure 6a,b). At higher magnification, graphite forms interconnected flakes concentrated along foliation planes and grain boundaries and locally occupies interstitial domains between quartz and muscovite (Figure 6b). These microstructural relationships provide evidence for deformation-assisted redistribution, recrystallization, and local coarsening of graphite during metamorphism. Quartz forms subhedral to anhedral grains occupying interstitial spaces within the graphite–mica matrix, whereas muscovite occurs as elongate platy crystals defining the dominant schistosity. Pyrrhotite occurs as a minor, locally disseminated phase associated with graphite in the ore-zone samples (Figure 6c,d).

The EDX spectra provide localized chemical information that complements the high-resolution BSE observations (Figure 7a–d). Spectra obtained from graphite-rich domains are characterized by dominant carbon (C) peaks with minor silicon (Si) contributions (Figure 7a). Mica-rich areas show prominent O, Al, Si, and K peaks, together with variable

Mg, Fe, and Ti (Figure 7b). A minor K peak is also present in the EDX spectrum; however, its non-diagnostic character does not permit definitive identification of K-feldspar based on EDX chemistry alone. Fe- and S-rich EDX spectra, characterized by prominent Fe and S peaks, provide chemical support for the presence of pyrrhotite in the analyzed ore-zone samples (Figure 7c,d).

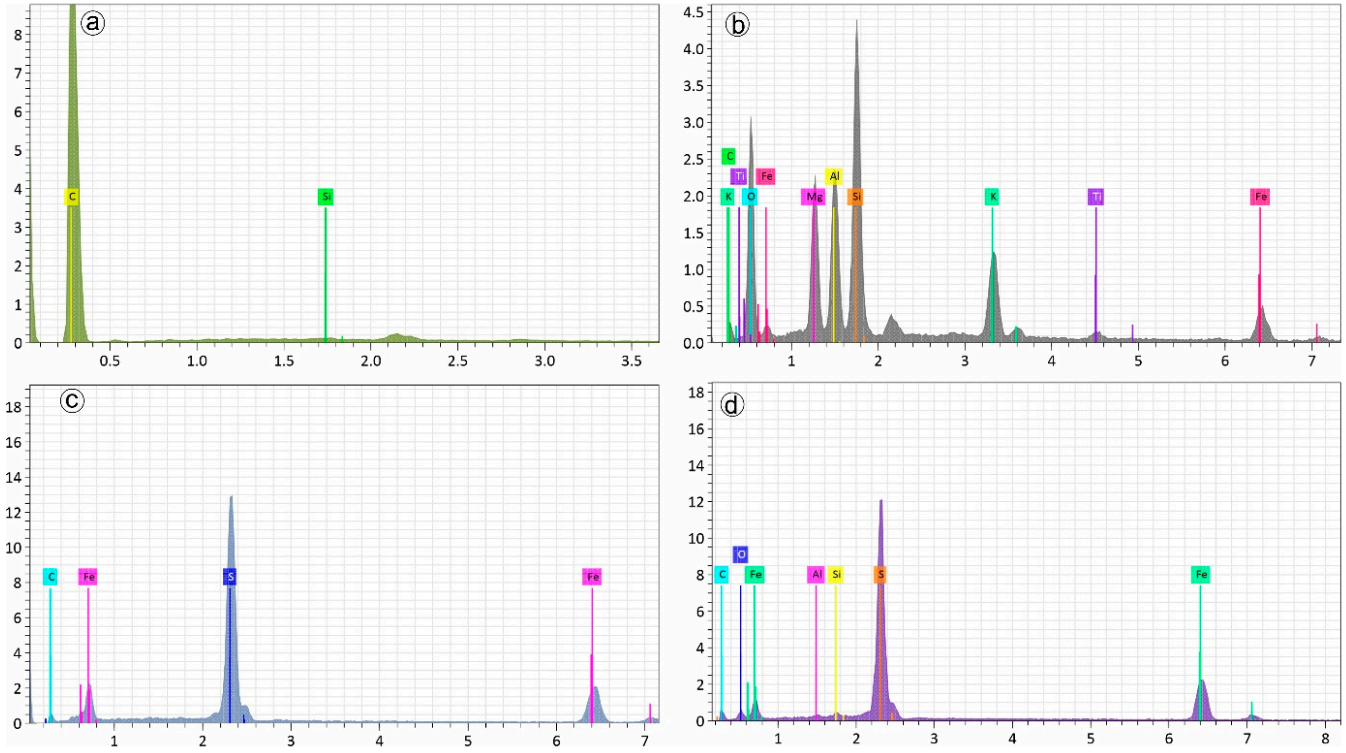


Figure 7. Representative EDX spectra of mineral phases from the Kambale Graphite Deposit, Wa-Lawra Belt, Ghana: (**a**) graphite showing a dominant carbon peak with minor silicon derived from adjacent quartz, (**b**) muscovite characterized by K-Al-Si-O peaks with minor Fe, Mg, and Ti, (**c**) pyrrhotite exhibiting strong Fe and S peaks indicative of iron sulfide composition, and (**d**) mixed pyrrhotite-silicate spectrum showing Fe-S peaks together with Al and Si from associated quartz–muscovite matrix minerals. The spectra confirm the mineral assemblage identified by SEM imaging and demonstrate the close association between graphite, silicates, and sulfide phases.

Overall, the SEM-BSE and EDX data provide information beyond the mineral identifications established by optical microscopy by resolving fine-scale graphite textures, mineral–mineral contacts, grain-boundary relationships, and the localized distribution of pyrrhotite, while EDX provides supporting chemical information for selected mineral phases. These observations show that graphite mineralization is hosted within a quartz–muscovite graphitic schist composed of abundant flake graphite, quartz, muscovite, and minor pyrrhotite. The observed microstructural relationships are consistent with deformation-assisted graphite recrystallization, redistribution, and local grain coarsening during regional metamorphism.

4.3. Whole-Rock Geochemistry

4.3.1. Major Element Variation

The metagranodiorite sample (SW1) is characterized by 64.59 wt.% SiO_2, 16.19 wt.% Al_2O_3, 5.05 wt.% Fe_2O_3, 2.24 wt.% MgO, 3.34 wt.% CaO, and 2.23 wt.% K_2O (Table 1). On the variation diagrams (Figure 8a–f), the metagranodiorite occupies an intermediate position between the graphite schists and gneisses and generally follows the compositional trends defined by the gneiss samples.

Table 1. Whole-rock geochemical composition of the studied rocks in the Kambale Graphite Deposit (Ag measured in ppb and S in %).

Sample ID	SW1	MSW-1	ASG-2M	GP1	GP2	GP3	GP3-B	GP3-C	GP3-E	GP4-1	GW1	GW2	GW4	GW5	GW6
Rock Type	**Metagranodiorite**	**Graphite Schist**	**Graphite Schist**	**Gneiss**	**Gneiss**	**Gneiss**	**Gneiss**	**Gneiss**	**Gneiss**	**Gneiss**	**Gneiss**	**Gneiss**	**Gneiss**	**Gneiss**	**Gneiss**
Major Oxides (wt.%)															
SiO_2	64.59	60.60	52.10	66.88	75.46	73.98	71.76	65.38	75.11	70.66	74.34	75.01	63.42	65.57	65.56
Al_2O_3	16.19	16.77	13.67	15.14	15.09	15.18	16.62	14.81	15.45	15.63	14.88	14.90	16.83	15.79	15.17
Fe_2O_3	5.05	7.39	4.97	5.37	0.75	1.08	1.11	6.35	0.77	2.38	1.02	0.87	4.61	5.10	5.86
MgO	2.24	1.80	0.71	1.95	0.13	0.35	0.38	2.83	0.13	1.09	0.38	0.18	2.01	1.97	2.41
CaO	3.34	4.63	1.87	2.49	1.46	3.02	3.56	2.69	1.21	3.41	3.27	1.93	3.34	3.30	2.13
Na_2O	4.01	3.98	0.01	3.88	4.10	4.76	5.24	2.99	3.57	4.53	4.69	4.80	4.18	3.91	3.79
K_2O	2.23	2.34	0.09	1.78	1.48	0.56	0.43	2.48	2.07	1.01	0.46	1.00	2.84	2.08	2.75
TiO_2	0.79	0.98	0.44	0.62	0.03	0.13	0.13	0.60	0.03	0.44	0.14	0.06	0.76	0.77	0.54
P_2O_5	0.25	0.24	0.02	0.15	0.02	0.03	0.02	0.18	0.02	0.01	0.02	0.02	0.38	0.20	0.26
MnO	0.06	0.06	20.10	0.22	0.05	0.01	0.02	0.10	0.01	0.01	0.01	0.01	0.07	0.05	0.09
Cr_2O_3	0.00	0.02	0.01	0.02	0.00	0.00	0.00	0.03	0.00	0.01	0.00	0.00	0.01	0.00	0.01
LOI	0.90	1.00	5.70	1.20	1.30	0.70	0.50	1.30	1.40	0.60	0.60	1.00	1.00	0.90	1.20
Total	99.91	99.89	99.81	99.91	99.98	99.96	99.94	99.90	99.95	99.95	99.97	99.97	99.90	99.90	99.91
Trace Elements (ppm)															
Mo	0.83	2.42	1.36	2.98	0.90	1.10	1.39	1.27	0.83	1.49	0.97	1.67	0.88	1.08	1.01
Cu	3.20	65.40	218	21.50	8.00	0.60	0.60	24.60	4.50	0.90	0.50	5.90	13.50	15.30	14.20
Pb	6.24	7.55	1.19	6.09	6.38	8.64	7.43	6.94	8.51	4.45	5.76	6.61	11.72	6.15	5.49
Zn	104.60	60.50	514	62.70	6.20	20.60	18.60	66.00	6.70	39.60	15.40	8.60	80.60	82.80	98.30
Ag	<20.00	74.00	83.00	33.00	<20.00	<20.00	<20.00	<20.00	<20.00	<20.00	<20.00	<20.00	<20.00	<20.00	<20.00
Co	7.90	17.60	35.90	11.30	0.30	2.80	1.90	14.60	0.30	5.40	2.00	1.40	8.30	8.80	12.80
Mn	434	449	>10,000	832	293	103	129	732	108	114	51	83	527	360	736
As	<0.20	0.30	0.40	0.40	0.30	0.50	0.30	<0.20	0.50	<0.20	<0.20	<0.20	<0.20	0.80	0.30
U	0.50	1.40	0.90	0.50	0.20	0.40	0.20	0.60	0.40	0.10	0.30	0.60	0.90	0.70	0.40
Th	1.40	3.70	1.60	0.80	0.80	1.00	0.60	2.20	1.70	0.10	0.30	1.70	5.50	3.80	0.80
Cd	<0.02	0.03	1.41	<0.02	<0.02	<0.02	<0.02	0.03	<0.02	<0.02	<0.02	<0.02	<0.02	<0.02	<0.02
Sb	<0.02	0.10	0.04	<0.02	<0.02	<0.02	<0.02	<0.02	<0.02	<0.02	<0.02	<0.02	<0.02	0.04	<0.02
Bi	<0.04	0.25	0.07	<0.04	<0.04	<0.04	<0.04	<0.04	<0.04	<0.04	<0.04	<0.04	<0.04	<0.04	<0.04
V	68.00	177	101	96.00	2.00	10.00	13.00	114	3.00	38.00	15.00	6.00	70.00	78.00	97.00
Cr	13.00	101	49.00	135.0	4.00	5.00	6.00	192	3.00	22.00	5.00	6.00	31.00	15.00	55.00
Ba	933	550	984	628	475	332	254	482	1770	412	237	710	1837	892	587
W	0.20	0.70	0.40	0.40	0.20	0.20	0.10	0.20	0.50	0.20	0.10	0.30	0.20	0.20	0.20
Sn	1.70	1.20	1.70	0.40	0.40	0.20	0.10	0.40	0.50	0.20	0.10	0.30	1.00	1.40	0.50
Be	<1.00	2.00	3.00	<1.00	<1.00	<1.00	<1.00	<1.00	<1.00	<1.00	<1.00	<1.00	2.00	<1.00	<1.00
Sc	6.90	21.50	10.80	11.00	1.60	1.00	0.80	14.30	1.60	1.50	0.70	2.20	6.20	9.10	11.90
S	<0.04	<0.04	<0.04	<0.04	<0.04	<0.04	<0.04	<0.04	<0.04	<0.04	<0.04	<0.04	<0.04	<0.04	<0.04
Y	8.00	20.30	27.70	6.50	1.80	1.30	0.70	5.60	2.80	0.60	0.70	1.70	4.80	8.90	10.10
Hf	3.42	2.09	1.80	2.80	0.42	2.92	0.94	2.40	0.65	1.14	2.30	1.02	4.43	3.62	1.48
Li	34.40	43.90	102	26.40	3.00	6.80	5.10	28.80	3.50	14.90	5.90	3.10	18.90	27.10	33.80

Table 1. *Cont.*

Sample ID	SW1	MSW-1	ASG-2M	GP1	GP2	GP3	GP3-B	GP3-C	GP3-E	GP4-1	GW1	GW2	GW4	GW5	GW6
Rock Type	**Metagranodiorite**	**Graphite Schist**	**Graphite Schist**	**Gneiss**	**Gneiss**	**Gneiss**	**Gneiss**	**Gneiss**	**Gneiss**	**Gneiss**	**Gneiss**	**Gneiss**	**Gneiss**	**Gneiss**	**Gneiss**
Rb	72.70	79.00	2.40	59.20	29.70	11.90	6.00	73.40	29.70	21.60	9.50	20.70	59.70	57.90	114
Ta	0.20	0.60	0.30	0.20	<0.10	<0.10	<0.10	0.30	<0.10	<0.10	<0.10	0.20	0.20	0.40	0.20
Nb	4.96	8.94	4.79	3.37	2.65	0.90	0.81	4.42	2.13	0.31	0.21	2.12	4.99	6.69	4.26
Cs	8.80	5.60	1.30	5.70	0.20	0.50	0.50	4.50	0.20	4.40	0.60	0.20	2.10	2.70	7.00
Ga	20.05	17.12	20.68	15.85	15.12	13.90	13.26	15.40	14.99	14.29	12.92	15.02	21.33	16.25	17.56
In	0.05	0.05	0.05	0.03	0.02	<0.01	<0.01	0.04	0.03	<0.01	<0.01	0.02	0.03	0.04	0.03
Re	<0.002	<0.002	<0.002	<0.002	<0.002	<0.002	<0.002	<0.002	<0.002	<0.002	<0.002	<0.002	<0.002	<0.002	<0.002
Se	<0.30	<0.30	0.60	<0.30	<0.30	<0.30	<0.30	<0.30	<0.30	<0.30	<0.30	<0.30	<0.30	<0.30	<0.30
Te	<0.05	<0.05	0.14	0.09	<0.05	0.07	0.08	0.08	<0.05	0.06	0.07	<0.05	0.14	<0.05	<0.05
Tl	0.49	0.42	0.14	0.40	0.11	0.10	0.08	0.45	0.10	0.21	0.07	0.08	0.43	0.36	0.77
Ni	20.00	37.00	111	32.00	20.00	20.00	20.00	38.00	20.00	20.00	20.00	20.00	20.00	20.00	25.00
Sr	576	252	90.00	480	286	794	818	433	292	646	694	406	1305	565	297
Zr	202	163	84.00	181	12.00	146	60.00	127	16.00	126	138	59.00	276	212	82.00
Rare Earth Elements (REE) (ppm)															
La	9.30	16.90	6.00	6.60	5.50	6.40	3.70	10.50	12.20	1.40	3.90	13.80	31.50	12.90	7.20
Ce	21.92	38.37	20.69	14.75	11.85	12.78	8.61	22.11	22.90	2.74	7.15	28.69	80.79	30.06	15.43
Pr	2.80	4.50	2.00	1.60	1.30	1.40	0.80	2.50	2.70	0.30	0.80	3.20	9.60	3.50	2.50
Nd	12.70	18.90	10.20	6.60	5.20	5.60	3.30	10.20	10.60	1.10	3.00	12.50	35.20	14.50	11.20
Sm	2.70	4.10	3.40	1.30	1.00	0.90	0.50	1.90	1.80	0.20	0.50	1.80	5.20	2.60	2.20
Eu	0.90	1.20	1.00	0.60	0.20	0.90	0.70	0.80	0.30	0.60	0.80	0.40	1.20	0.80	0.50
Gd	2.40	3.90	5.00	1.40	0.70	0.60	0.30	1.50	1.20	0.10	0.30	1.00	2.80	2.10	1.70
Tb	0.30	0.60	0.70	0.20	<0.10	<0.10	0.20	0.20	<0.10	<0.10	<0.10	<0.10	0.30	0.30	0.20
Dy	1.70	4.00	5.10	1.40	0.40	0.30	0.20	1.30	0.60	0.10	0.10	0.40	1.40	1.90	1.70
Ho	0.30	0.80	1.00	0.30	0.10	0.10	0.10	0.20	0.10	0.10	0.10	0.10	0.20	0.40	0.40
Er	0.80	2.50	3.00	0.70	0.20	0.10	0.10	0.70	0.30	0.10	0.10	0.20	0.50	1.10	1.10
Tm	0.10	0.40	0.40	0.10	0.10	0.10	0.10	0.10	0.10	0.10	0.10	0.10	0.10	0.10	0.20
Yb	0.80	2.60	2.60	0.80	0.20	0.10	0.10	0.70	0.30	0.10	0.10	0.10	0.40	1.00	1.10
Lu	0.10	0.40	0.40	0.10	0.10	0.10	0.10	0.10	0.10	0.10	0.10	0.10	0.10	0.20	0.20
∑REE	56.82	99.17	61.49	36.45	26.85	29.38	18.81	52.81	53.20	7.04	17.05	62.39	169.29	71.46	45.63
∑LREE	49.42	82.77	42.29	30.85	24.85	27.08	16.91	47.21	50.20	5.74	15.35	59.99	162.29	63.56	38.53
∑MREE	5.30	9.70	11.80	3.60	1.30	1.80	1.40	3.80	2.10	0.80	1.20	1.80	5.70	5.10	4.10
∑HREE	2.10	6.70	7.40	2.00	0.70	0.50	0.50	1.80	0.90	0.50	0.50	0.60	1.30	2.80	3.00
LREE/HREE	23.53	12.35	5.71	15.43	35.50	54.16	33.82	26.23	55.78	11.48	30.70	99.98	124.84	22.70	12.84
$(La/Yb)_N$	7.90	4.42	1.57	5.60	18.68	43.48	25.14	10.19	27.63	9.51	26.49	93.75	53.50	8.76	4.45
$(La/Sm)_N$	2.15	2.57	1.10	3.17	3.44	4.44	4.62	3.45	4.23	4.37	4.87	4.79	3.78	3.10	2.04
$(Gd/Yb)_N$	2.43	1.21	1.56	1.42	2.83	4.85	2.43	1.73	3.24	0.81	2.43	8.09	5.66	1.70	1.25
$(Ce/Yb)_N$	7.20	3.88	2.09	4.84	15.56	33.57	22.61	8.30	20.05	7.20	18.78	75.35	53.05	7.90	3.68
Eu/Eu*	1.08	0.92	0.74	1.36	0.73	3.73	5.51	1.44	0.62	12.93	6.30	0.91	0.96	1.04	0.79
Ce/Ce*	1.04	1.06	1.45	1.10	1.07	1.03	1.21	1.04	0.97	1.02	0.98	1.04	1.12	1.08	0.88
Dy_N/Yb_N	1.39	1.01	1.28	1.15	1.31	1.96	1.31	1.22	1.31	0.65	0.65	2.62	2.29	1.24	1.01

Eu/Eu* and Ce/Ce* represent the europium (Eu) and cerium (Ce) anomalies, respectively.

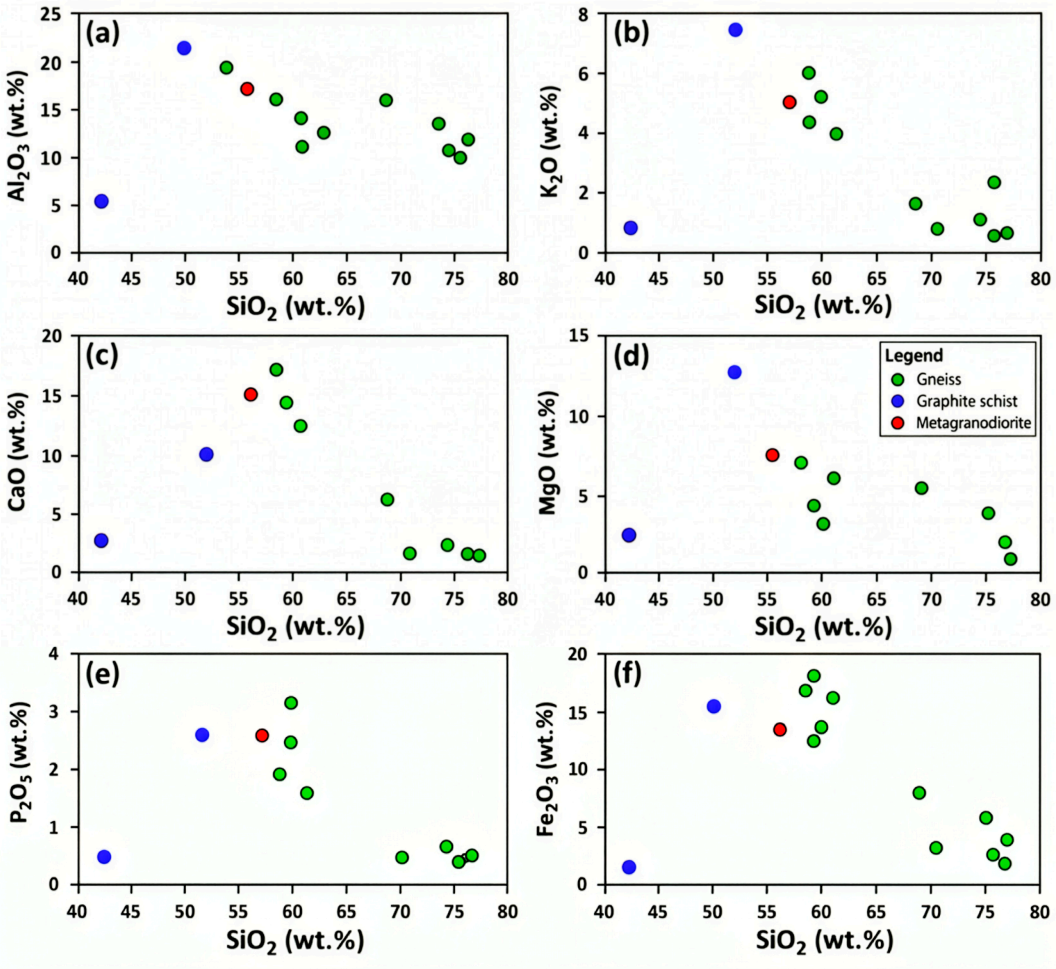


Figure 8. Harker variation diagrams showing the relationships between SiO_2 and selected major oxides in the metagranodiorite, graphite schists, and gneisses from the study area: (**a**) SiO_2 versus Al_2O_3, (**b**) SiO_2 versus K_2O, (**c**) SiO_2 versus CaO, (**d**) SiO_2 versus MgO, (**e**) SiO_2 versus P_2O_5, and (**f**) SiO_2 versus Fe_2O_3.

The graphite schists are distinguished by the lowest silica contents (52.10–60.60 wt.% SiO_2) and the highest concentrations of several major oxides (Table 1). They contain 13.67–16.77 wt.% Al_2O_3, 4.97–7.39 wt.% Fe_2O_3, 0.71–1.80 wt.% MgO, 1.87–4.63 wt.% CaO, and 0.44–0.98 wt.% TiO_2 (Table 1). On the variation diagrams (Figure 8a–f), the graphite schists define the low-SiO_2 end of the trends and are enriched in Fe_2O_3, MgO, CaO, and P_2O_5 relative to the other lithologies. Their position suggests a greater abundance of ferromagnesian and accessory minerals compared with the silica-rich rocks.

The gneisses constitute the dominant lithology and display the widest compositional range. They contain 63.42–75.46 wt.% SiO_2, 14.81–16.83 wt.% Al_2O_3, 0.75–6.35 wt.% Fe_2O_3, 0.13–2.83 wt.% MgO, 1.21–3.56 wt.% CaO, 2.99–5.24 wt.% Na_2O, and 0.43–2.84 wt.% K_2O (Table 1). In the variation diagrams (Figure 8a–f), the gneisses define most of the observed trends and show a progressive decrease in Fe_2O_3, MgO, CaO, and P_2O_5 with increasing SiO_2. The highest-silica gneisses (>70 wt.% SiO_2) are characterized by particularly low Fe_2O_3 (<2.5 wt.%), MgO (<1.1 wt.%), and P_2O_5 (<0.05 wt.%).

The Harker variation diagrams (Figure 8a–f) illustrate compositional differences among the graphite schists, metagranodiorite, and gneisses. The graphite schists generally occupy the lower SiO_2 range and are characterized by relatively higher Fe_2O_3, MgO, CaO, and P_2O_5 contents compared with most of the gneiss samples. The gneisses span a wider range of SiO_2 contents and generally show decreasing Fe_2O_3, MgO, CaO, and P_2O_5

contents with increasing SiO_2. The metagranodiorite sample plots within the broader compositional ranges defined by the other lithologies, although its position varies among the individual diagrams. Al_2O_3 and K_2O show greater scatter and do not exhibit a consistent linear relationship with SiO_2, particularly among the gneisses. Overall, the major-element variation diagrams highlight compositional heterogeneity and systematic differences in major-element distributions among the studied lithologies.

4.3.2. Trace Element Characteristics

The metagranodiorite (SW1) is characterized by moderate concentrations of large-ion lithophile elements (LILEs) and relatively low concentrations of transition metals. The sample contains 538–576 ppm Sr, 933–993 ppm Ba, 72.7 ppm Rb, 134–202 ppm Zr, and 4.96–5.00 ppm Nb. Transition metal concentrations are generally low, with Cu (3.2 ppm), Ni (7.4–20 ppm), Co (7.9 ppm), Cr (13 ppm), and V (68 ppm) (Table 1). Uranium and thorium contents are low (0.5 ppm U and 1.4 ppm Th).

The graphite schists (MSW-1 and ASG-2M) show marked enrichment in several trace elements compared to the other lithologies. Concentrations of Cu (65.4–218 ppm), Zn (60.5–514 ppm), Ag (74–83 ppb), Ni (31.2–145 ppm), Co (17.6–35.9 ppm), Cr (49–101 ppm), V (101–177 ppm), and Li (43.9–102 ppm) are significantly elevated (Table 1). The highest values of Cu (218 ppm), Zn (514 ppm), Ag (83 ppb), Mn (>10,000 ppm), Ni (145 ppm), and Li (102 ppm) occur in sample ASG-2M (Table 1). Large-ion lithophile element contents range from 236–252 ppm Sr, 550–582 ppm Ba, and 2.4–79 ppm Rb, whereas high-field-strength elements (HFSE) remain relatively low, with 79.9–163 ppm Zr and 4.79–8.94 ppm Nb (Table 1).

The gneisses exhibit a wider compositional range than the metagranodiorite and generally lower concentrations of transition metals than the graphite schists. Copper varies from 0.5 to 24.6 ppm, Zn from 6.2 to 98.3 ppm, Ni from 1.3 to 38 ppm, Co from 0.3 to 14.6 ppm, and Cr from 3 to 192 ppm (Table 1). The gneisses are characterized by variable enrichments in the LILEs, including Sr (274–1305 ppm), Ba (237–1868 ppm), and Rb (6.0–114 ppm) (Table 1). HFSE concentrations show considerable variability, with Zr ranging from 12 to 276 ppm, Y from 3 to 13 ppm, and Nb from 0.21 to 7 ppm (Table 1).

Despite the localized occurrence of pyrrhotite in the ore-zone samples examined by SEM-BSE/EDX, whole-rock sulfur concentrations are uniformly low (<0.04 wt.%) across the analyzed samples (Table 1), indicating that sulfur-bearing minerals constitute only a minor proportion of the bulk rock.

Primitive mantle-normalized multi-element patterns for the graphite schists, metagranodiorite, and gneisses exhibit broadly similar overall distributions, although the magnitude of enrichment varies among samples (Figure 9a). The patterns are characterized by enrichment in Th, U, light rare earth element (LREE)-related components relative to Nb, Ta, Ti, and the heavy rare earth element (HREE) segment. Graphite schists generally display higher normalized abundances of Th and LREEs than most gneiss samples, whereas the metagranodiorite exhibits an intermediate pattern. Negative Nb-Ta and Ti anomalies are present in most samples regardless of lithology (Figure 9a). The HREE segment, represented by Dy, Ho, Er, Tm, Yb, Lu, and Y, is comparatively less fractionated and displays relatively uniform normalized abundances. Variations in the degree of trace-element enrichment are most pronounced among the gneiss samples, which exhibit a wider compositional range than the graphite schists and metagranodiorite. The graphite schists are characterized by comparatively smooth trace-element profiles with moderate to strong enrichment of incompatible elements.

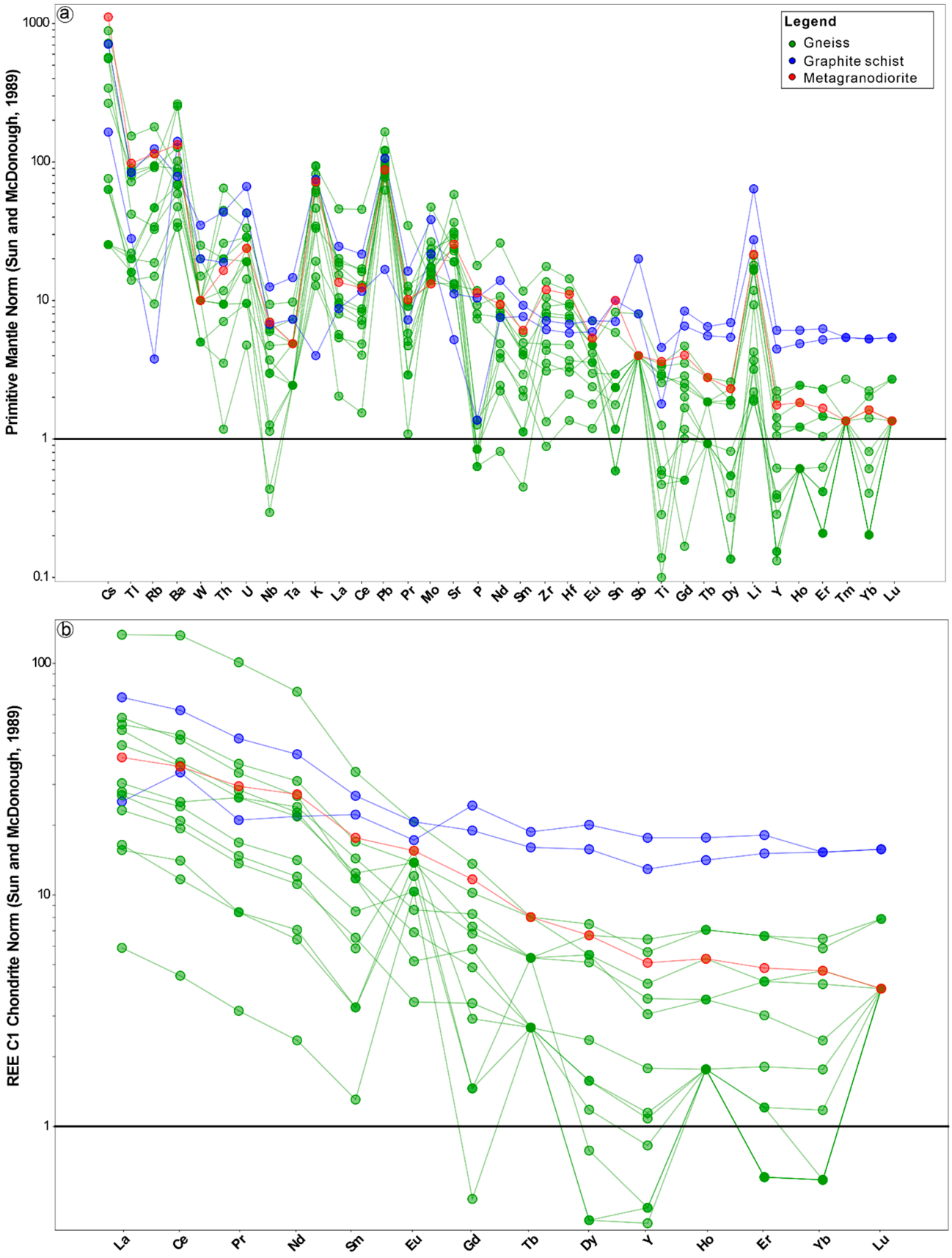


Figure 9. Trace and rare earth element patterns of the studied rocks: (**a**) primitive mantle-normalized trace element patterns, and (**b**) chondrite-normalized REE patterns for graphite schists, gneisses, and metagranodiorite from the Kambale Graphite Deposit, Wa-Lawra Belt, Ghana. Normalization values are from [29].

In contrast, the gneisses show greater variability in normalized trace-element abundances, whereas the metagranodiorite displays a pattern broadly similar to that of the graphite schists but with lower overall enrichment levels for several incompatible elements. Therefore, the primitive mantle-normalized patterns indicate systematic differences in trace-element abundances among the three lithological groups while maintaining similar general pattern shapes (Figure 9a).

4.3.3. Rare Earth Element Patterns

The metagranodiorite contains a moderate total REE concentration (ΣREE = 56.82 ppm) and is characterized by enrichment of light rare earth elements (LREE) relative to heavy rare earth elements (HREE) (ΣLREE = 49.42 ppm; ΣHREE = 2.10 ppm). The LREE/HREE ratio of 23.53 and $(La/Yb)_N$ value of 7.90 indicate pronounced LREE enrichment. The sample exhibits a near-neutral europium anomaly (Eu/Eu^* = 1.08) and a weak positive cerium anomaly (Ce/Ce* = 1.04).

The graphite schists display moderate to high REE abundances, with ΣREE values ranging from 61.49 to 99.17 ppm (Table 1). Total ΣLREE concentrations vary from 42.29 to 82.77 ppm, whereas HREE contents range from 6.70 to 7.40 ppm (Table 1). The graphite schists show lower LREE/HREE ratios (5.71–12.35) and lower $(La/Yb)_N$ values (1.57–4.42) than most gneisses, indicating comparatively flatter REE patterns (Table 1). They display weak to moderate negative europium anomalies (Eu/Eu^* = 0.74–0.92) and slight positive cerium anomalies (Ce/Ce^* = 1.06–1.45) (Table 1).

The gneisses exhibit the largest variation in REE compositions. Total REE concentrations range from 7.14 to 169.29 ppm, with corresponding ΣLREE values of 5.74–162.29 ppm and ΣHREE values of 0.50–3.00 ppm (Table 1). Most gneisses are strongly enriched in LREEs relative to HREEs, as indicated by high LREE/HREE ratios (11.48–124.84) and elevated $(La/Yb)_N$ values (4.45–93.75) (Table 1). Sample GW4 exhibits the highest REE enrichment (ΣREE = 169.29 ppm), whereas GP4–1 records the lowest value (ΣREE = 7.14 ppm) (Table 1). Europium anomalies are highly variable, ranging from negative (Eu/Eu* = 0.62) to strongly positive (Eu/Eu* = 12.93), while cerium anomalies are generally weak (Ce/Ce* = 0.88–1.21) (Table 1). The generally high LREE/HREE ratios indicate strong fractionation and preferential enrichment of light rare earth elements.

Chondrite-normalized REE patterns of the Kambale Graphite Deposit (Figure 9b) are characterized by enrichment of light rare earth elements (LREEs) relative to heavy rare earth elements (HREEs). The graphite schists display moderately fractionated REE patterns with LaN/Yb_N ratios of approximately 4 to 6. Their REE profiles are relatively smooth and show elevated concentrations throughout the REE spectrum. Total REE abundances are generally higher than those observed in most gneiss samples. The graphite schists exhibit weak to moderate negative Eu anomalies and relatively flat HREE segments from Ho to Lu.

The metagranodiorite samples show REE patterns similar to those of the graphite schists, with strong LREE enrichment and a gradual decrease toward the HREEs. Negative Eu anomalies are present, and HREE abundances remain relatively uniform from Ho to Lu. The overall REE concentrations are intermediate between those of the graphite schists and the more enriched gneiss samples.

The gneisses display the widest range of REE abundances and fractionation patterns. Most samples are enriched in LREEs relative to HREEs and show decreasing concentrations from La to Lu. Several samples exhibit pronounced negative Eu anomalies, whereas others display only weak Eu depletion. HREE concentrations are generally low and relatively flat, although some samples show marked depletion from Dy to Lu. A few gneiss samples are strongly enriched in LREEs, reaching chondrite-normalized La values exceeding 100, while others possess comparatively lower overall REE abundances.

4.4. Total Carbon Content (%C) and Carbon Isotope Composition of Graphite Schist Samples from the Ore Zone

The total carbon contents (%C) of the graphite schists in the ore zone range from 0.58 to 17.29 wt.% (Table 2), with an average of 8.42 wt.%. The highest carbon contents occur in ASG 4-3 (17.29 wt.%), ASG 4-2-2 (15.59 wt.%), MSGW (14.05 wt.%), and MSGW-1 (13.82 wt.%), whereas ASG-1 records the lowest value (0.58 wt.%). The $\delta^{13}C$ values range from −31.83‰ to −24.33‰ (VPDB) (Table 2), with an average of −28.92‰. The most negative $\delta^{13}C$ value occurs in ASG 4-1 (−31.83‰), whereas ASG-1 records the least negative value (−24.33‰). Samples with relatively high total carbon contents generally exhibit more negative $\delta^{13}C$ values, with most carbon-rich samples (>8 wt.% C) showing $\delta^{13}C$ values between −31.83‰ and −27.29‰.

Table 2. Total carbon content (%C) and carbon isotope composition of graphite schists from the Kambale Graphite Deposit.

Sample ID	Rock Type	%C	$\delta^{13}C$
MICA GX Schist-1	Graphite schist	1.72	−26.78
GF	Graphite schist	0.96	−26.36
ASU	Graphite schist	3.96	−24.70
MS GIF CAR	Graphite schist	4.67	−26.76
ASG-1	Graphite schist	0.58	−24.33
ASG 4-4	Graphite schist	10.93	−31.57
ASG 4-2	Graphite schist	1.09	−30.02
ASG 4-1	Graphite schist	12.67	−31.83
MSGW	Graphite schist	14.05	−27.29
MSGW-1	Graphite schist	13.82	−27.85
ASG 4-2-2	Graphite schist	15.59	−31.00
ASG 4-3	Graphite schist	17.29	−31.57
ASGC-3	Graphite schist	10.49	−31.33
ASGS-1	Graphite schist	8.40	−31.13
ASG 4	Graphite schist	10.09	−31.32

5. Discussion

5.1. Nature and Protolith of the Gneisses and Metagranodiorite

The whole-rock geochemical data support a granitoid affinity for the gneisses and the analyzed metagranodiorite at Kambale (Figure 10a,b). The samples plot predominantly within the granite and granodiorite fields on the total alkali–silica diagram, while most samples are peraluminous on the A/CNK versus A/NK diagram (Figure 10a,b). These characteristics are consistent with felsic granitoid protoliths and suggest a significant crustal contribution [30].

The gneisses exhibit a broader range of SiO_2 and alkali contents than the analyzed metagranodiorite, although the two lithologies show considerable compositional overlap. This variability may reflect differences among the original granitoid precursors and/or modification during subsequent metamorphism. The preservation of relict igneous characteristics identified petrographically, together with the broadly overlapping geochemical signatures, supports interpretation of the gneisses as orthogneisses derived from granitoid protoliths, whereas the metagranodiorite represents a less deformed granitoid-derived lithology.

The geochemical classification therefore provides evidence for a related felsic magmatic affinity among the granitoid-derived rocks at Kambale. However, classification of metamorphosed rocks using major-element compositions requires caution because metamorphism and fluid–rock interaction may modify some elemental abundances. Ac-

cordingly, the granitoid protolith interpretation is based on the agreement between the geochemical characteristics and the preserved petrographic evidence, rather than on the classification diagrams alone.

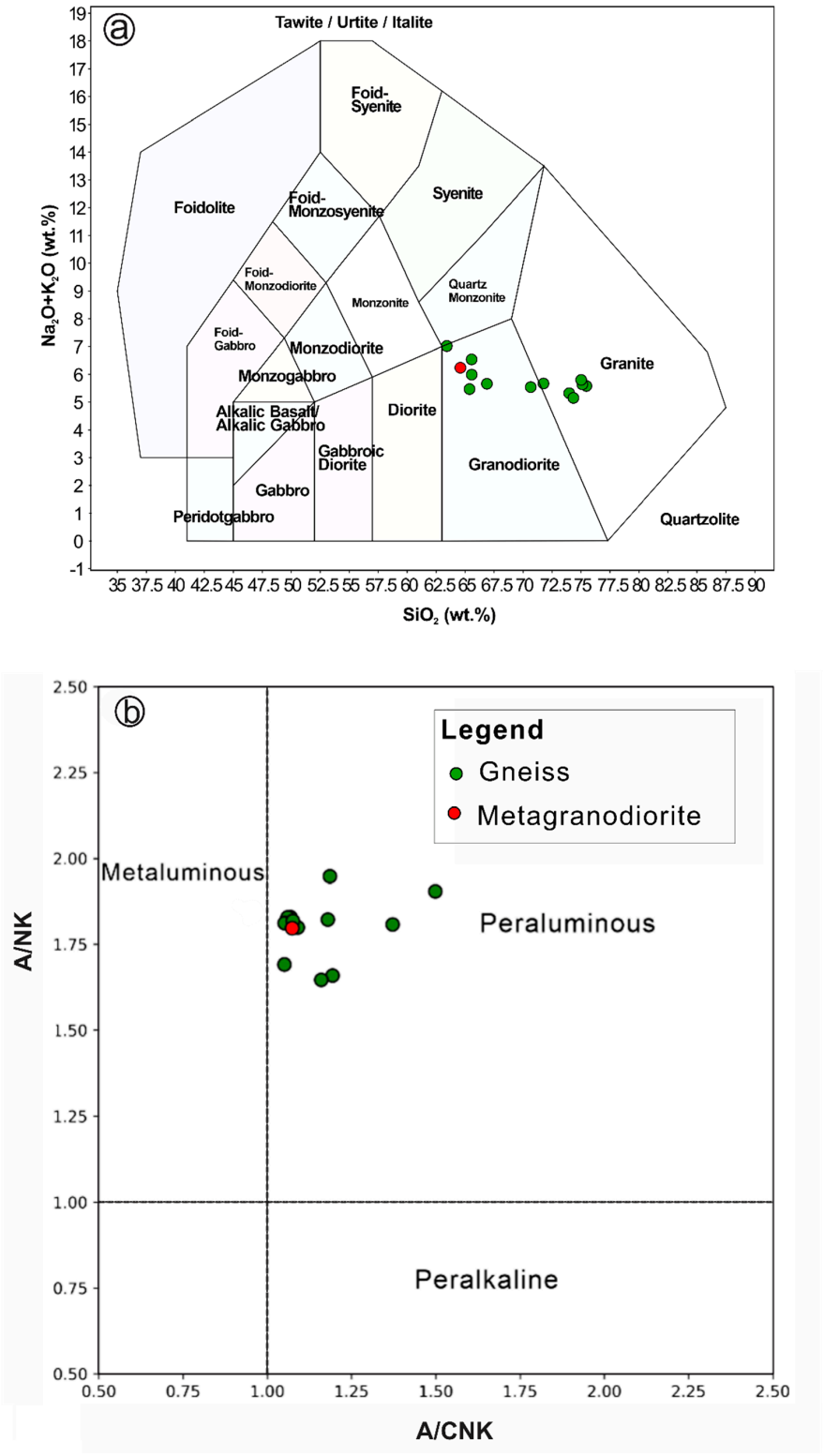


Figure 10. Geochemical classification and alumina saturation diagrams for the gneisses and metagranodiorite of the Kambale Graphite Deposit, Wa-Lawra Belt, Ghana: (**a**) Total alkali–silica (TAS) diagram indicating granitic to granodioritic protolith affinities; (**b**) A/NK versus A/CNK diagram showing predominantly peraluminous compositions and the involvement of evolved continental crustal material.

5.2. Paragenetic Evolution of the Kambale Graphite Deposit

The integrated geological, petrographic, geochemical, and stable carbon isotope evidence indicates that graphite mineralization at Kambale developed from a carbonaceous sedimentary precursor that was subsequently modified during regional metamorphism and deformation. The precursor succession is interpreted to have comprised quartz-rich clastic sediments interlayered with organic-rich pelitic horizons, consistent with the occurrence of graphite-rich schists and the widespread presence of quartz in the studied rocks [31,32].

During progressive regional metamorphism, the carbonaceous material was transformed into crystalline graphite, accompanied by development of the quartz–muscovite–graphite assemblage. Continued deformation promoted recrystallization, preferential alignment, and local coarsening of graphite along schistosity planes. The occurrence of graphite along grain boundaries and interstitial domains between quartz and muscovite is consistent with deformation-assisted redistribution and recrystallization of carbon [31,33]. These relationships indicate that the present graphite textures resulted from the interaction of metamorphic recrystallization and deformation rather than from simple preservation of the original sedimentary carbonaceous material.

Minor pyrrhotite represents a localized sulfide component of the graphite-bearing assemblage. Its occurrence in the ore-zone samples is supported by SEM-BSE/EDX observations, while the low whole-rock sulfur concentrations indicate that sulfide minerals constitute only a minor component of the bulk rock. Late-stage epidote locally overprints the principal metamorphic fabric, indicating limited retrograde re-equilibration during cooling. The relatively restricted development of retrograde minerals suggests that post-peak alteration did not substantially modify the graphite-bearing assemblage.

The resulting paragenetic sequence (Figure 11) therefore comprises sedimentation of an organic-rich precursor, regional metamorphic graphitization, deformation-assisted graphite recrystallization and local coarsening, minor pyrrhotite formation, and localized retrograde alteration. This sequence provides a genetic framework for the development of graphite mineralization at Kambale within the Paleoproterozoic tectono-metamorphic evolution of the Wa–Lawra Belt [23–25,31–33].

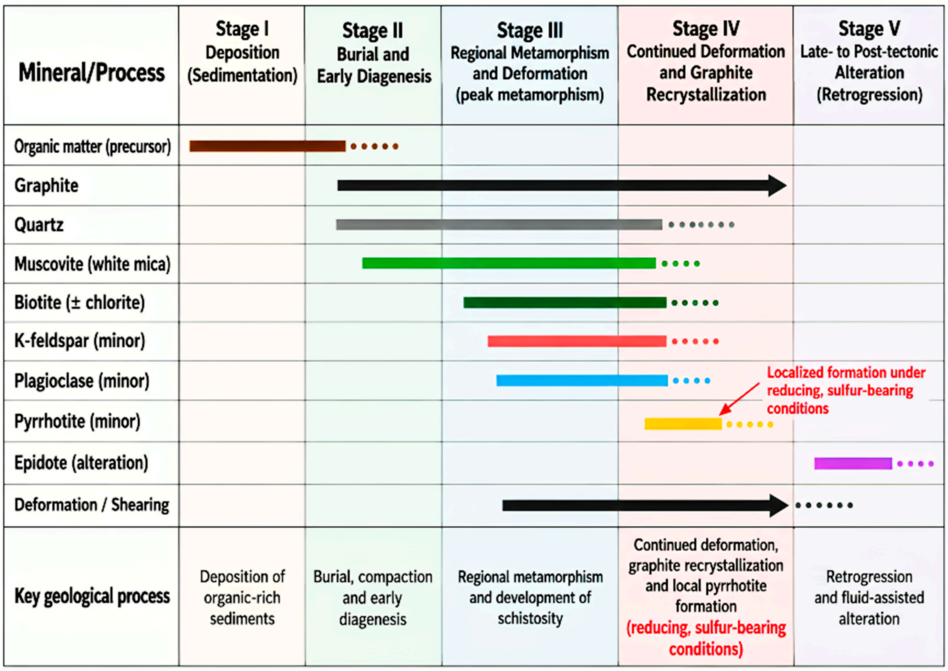


Figure 11. Proposed paragenetic sequence of the Kambale Graphite Deposit, Wa-Lawra Belt, Ghana.

5.3. Metamorphic Evolution of Graphite-Bearing Rocks

5.3.1. Mineralogical Evidence Based on Metamorphic Assemblages

Graphite crystallinity and structural ordering provide important constraints on the evolution of carbonaceous material during metamorphism. Quantitative parameters such as XRD *d*002 spacing, degree of graphitization (DOG), and Raman *I*D/*I*G ratios can be used to evaluate the structural ordering of graphite. However, such quantitative crystallinity data have not previously been reported for the Kambale Graphite Deposit or the Wa-Lawra Belt and were not determined in the present study. Consequently, graphite evolution is evaluated qualitatively using petrographic and SEM-BSE/EDX observations. The petrographic and SEM-BSE/EDX results indicate that the graphite-bearing rocks of the Kambale deposit underwent progressive regional metamorphism accompanied by deformation and recrystallization. The observed mineral assemblages and textural relationships record the transformation of sedimentary and igneous precursor rocks during Paleoproterozoic tectono-metamorphic events within the Wa-Lawra Belt. Such mineralogical and microstructural modifications are characteristic of graphitic terranes that have experienced medium- to high-grade regional metamorphism [4,10]. The metagranodiorite preserves relict igneous assemblages comprising quartz, plagioclase, K-feldspar, and hornblende, despite clear evidence of metamorphic overprinting. The development of undulose extinction in quartz, embayed grain boundaries, recrystallized quartz domains, and weak foliation indicates deformation under elevated temperatures during regional metamorphism [34]. Similar microstructures are widely regarded as indicators of subsolidus deformation and dynamic recrystallization in metamorphosed granitoids [35–37]. The coexistence of primary igneous minerals and recrystallized phases suggests incomplete textural re-equilibration, implying that metamorphism modified but did not completely obliterate the original granitoid fabric.

The gneisses exhibit a greater degree of metamorphic reworking than the metagranodiorite, as reflected by the abundance of recrystallized quartz, biotite, and epidote. The replacement of primary textures by fine-grained recrystallized aggregates indicates substantial mineral re-equilibration during progressive metamorphism. The presence of epidote inclusions within plagioclase and the widespread occurrence of biotite suggest extensive metamorphic modification under conditions favourable for hydrous mineral growth. Epidote-bearing assemblages commonly develop during prograde to retrograde metamorphism through hydration reactions involving feldspar-rich protoliths [38,39]. Similar mineral assemblages have been reported from metamorphosed granitoids subjected to amphibolite-facies metamorphism [40].

The graphite schists record the most intense metamorphic modification and deformation among the studied lithologies. The well-developed schistosity defined by aligned graphite flakes, muscovite, and quartz bands reflects extensive mineral recrystallization during regional metamorphism. The predominance of lepidoblastic textures and the fragmentation of muscovite porphyroblasts indicate deformation under ductile conditions. Such fabrics are characteristic of graphitic metapelites that have undergone significant tectonic shortening and metamorphic recrystallization [4,9]. The complete obliteration of primary sedimentary textures further suggests that the original carbonaceous sediments experienced substantial metamorphic transformation.

SEM-EDX observations provide additional evidence for the metamorphic origin of the graphite mineralization. Graphite occurs predominantly as fine crystalline flakes, with locally coarser flakes forming interconnected aggregates aligned parallel to the principal foliation and intimately associated with quartz and muscovite. The close association between graphite and muscovite suggests that graphite crystallization was closely linked to metamorphic fabric development, with muscovite forming the dominant foliation framework within which graphite flakes preferentially grew. Similar relationships have been docu-

mented in graphite deposits from Sri Lanka, Madagascar, Mozambique, and China, where graphite recrystallization accompanied mica growth during regional metamorphism [4,41].

The observed mineral assemblages and textures provide important constraints on the pressure-temperature conditions attained during metamorphism. The occurrence of hornblende in the metagranodiorite and biotite-bearing gneisses indicates temperatures above those associated with greenschist-facies metamorphism. Amphibole-bearing assemblages commonly develop at temperatures exceeding approximately 500 °C under moderate pressures and are typical of amphibolite-facies conditions [38,40].

Previous investigations of the Wa-Lawra Belt estimated peak metamorphic conditions of approximately 600–750 °C and pressures of 5–8 kbar [19]. These conditions are consistent with the extensive recrystallization observed in the graphite-bearing schists and the development of crystalline flake graphite. Experimental and natural studies have demonstrated that progressive ordering of carbonaceous material into crystalline graphite is strongly controlled by temperature and becomes increasingly efficient under amphibolite-facies conditions [4,7,41].

The preferential orientation of graphite flakes parallel to the foliation, together with local grain coarsening and recrystallized textures, indicates that graphite growth and reorganization occurred under elevated temperatures during regional deformation. Quartz grains exhibiting dynamic recrystallization and irregular grain boundaries further support syn-tectonic mineral growth and continued metamorphic re-equilibration under high-temperature conditions. Moreover, the close association of pyrrhotite with graphite, quartz, and muscovite, together with its enclosed occurrence within the graphite-bearing matrix, suggests that minor sulfide recrystallization accompanied regional metamorphism rather than resulting from a later hydrothermal overprint [42–44].

The quartz–muscovite–graphite mineral assemblage is consistent with medium-grade metamorphic conditions broadly corresponding to the lower amphibolite facies (approximately 500–600 °C) [39,40]. This temperature range is inferred from the preserved equilibrium mineral assemblage and should be regarded as a broad indication of the conditions recorded by the studied rocks rather than as an independent estimate of the regional metamorphic peak. The higher temperature range of 600–750 °C represents previously reported peak metamorphic conditions for the Wa-Lawra Belt [19]. The difference between these ranges may reflect the fact that the preserved mineral assemblage does not necessarily record the maximum regional temperature attained during metamorphism. Furthermore, the textural equilibrium and intimate intergrowth among graphite, pyrrhotite, quartz, and muscovite indicate that these minerals recrystallized contemporaneously during prograde metamorphism, reflecting metamorphic re-equilibration of the graphitic schist under regional metamorphic conditions [45]. This interpretation is further supported by the stable carbon isotope composition of the graphite-bearing carbonaceous material in the graphite schists, with $\delta^{13}C$ values ranging from −31‰ to −26‰ (VPDB). These relatively light isotopic values are consistent with a carbonaceous sedimentary precursor that underwent metamorphic transformation and graphitization rather than a predominantly mantle-derived or inorganic carbonate source [46–48]. The combined petrographic, mineralogical, and isotopic evidence therefore supports a sedimentary carbonaceous precursor that was subsequently transformed and recrystallized to form flake graphite during regional metamorphism.

5.3.2. Metamorphic Facies Determination from Mineralogy

The mineralogical and petrographic characteristics of the graphite-bearing rocks at Kambale indicate metamorphism predominantly under amphibolite-facies conditions. The principal mineral assemblages, comprising quartz, muscovite, biotite, hornblende, plagio-

clase, and K-feldspar, are consistent with amphibolite-facies metamorphism in aluminous metasedimentary and granitoid-derived rocks [38,40]. The preservation of hydrous minerals, particularly muscovite in the graphite schists and hornblende in the metagranodiorite, together with the absence of diagnostic granulite-facies minerals such as orthopyroxene and cordierite, suggests that granulite-grade metamorphism was not regionally pervasive [39,40]. This interpretation is consistent with regional studies identifying amphibolite-facies metamorphism as the dominant metamorphic grade within the Wa–Lawra Belt and adjacent Paleoproterozoic Birimian terranes [24,49,50].

The graphitic metasedimentary rocks are locally intruded by felsic pegmatitic and quartz–feldspar-rich bodies (Figure 1), indicating that sedimentation was followed by magmatic activity, while the metamorphic overprint is recorded by the mineral assemblages and metamorphic textures. Regional petrological and geochronological studies have estimated peak conditions of approximately 600–750 °C and 5–8 kbar for the Wa–Lawra Belt during the Eburnean Orogeny [50]. These regional estimates provide a broader tectonometamorphic context but should not be regarded as direct P–T estimates for the Kambale samples.

At Kambale, the preserved quartz–muscovite–graphite assemblage, together with crystalline flake graphite, extensive quartz recrystallization, and strong schistosity, is broadly consistent with lower amphibolite-facies conditions of approximately 500–600 °C. Graphite occurs predominantly as fine- to medium-crystalline flakes aligned parallel to the penetrative foliation and intimately associated with recrystallized quartz and muscovite, reflecting progressive graphitization and metamorphic recrystallization [7,41]. Locally, individual flakes or aggregates are relatively coarser. SEM-BSE and EDX observations further show graphite along foliation planes, grain boundaries, and interstitial domains between quartz and muscovite, indicating deformation-assisted recrystallization and local concentration of carbon during metamorphism. The intimate association of graphite with quartz, muscovite, and minor pyrrhotite is consistent with syn-metamorphic recrystallization during the Eburnean tectonometamorphic evolution of the Wa–Lawra Belt [10,33,41,51].

Collectively, the mineralogical, petrographic, and microtextural evidence indicates that the Kambale graphite-bearing rocks predominantly record lower amphibolite-facies metamorphism. These conditions were sufficient to promote graphitization, quartz recrystallization, foliation development, and deformation-assisted graphite recrystallization, resulting in the crystalline flake graphite mineralization observed at the deposit.

5.4. Petrogenesis and Tectonic Setting

5.4.1. Geochemical Characteristics of the Granitoid Protoliths

The geochemical characteristics of the graphite-bearing rocks provide important constraints on the nature of the source materials that supplied sediments to the Kambale depositional basin. The relatively high SiO_2 and Al_2O_3 contents of the graphite schists, together with their generally low MgO and TiO_2 contents, are consistent with a dominant contribution from felsic continental crustal sources. Felsic-derived sediments are typically characterized by abundant quartz and feldspar-derived components, resulting in relatively high SiO_2 and Al_2O_3 contents compared with sediments derived predominantly from mafic sources [11,12].

The primitive mantle-normalized trace-element patterns further support this interpretation. The graphite schists and associated gneisses display enrichment in large ion lithophile elements (LILEs), including Rb, Ba, K, and Th, together with pronounced negative Nb and Ti anomalies. Such geochemical signatures are characteristic of felsic upper continental crust-derived sediments and are commonly observed in metasedimentary rocks derived from evolved continental sources [11,12]. The negative Nb-Ti anomalies indicate

depletion of high-field-strength elements relative to LILEs and are generally associated with felsic magmatic sources and continental arc-derived sediments.

The REE patterns also indicate strong felsic provenance. The studied rocks are characterized by enrichment of light rare earth elements (LREEs) relative to heavy rare earth elements (HREEs), with elevated LREE/HREE and $(La/Yb)_N$ ratios. Such fractionated REE patterns are typical of sediments derived from granitic to granodioritic source rocks because felsic rocks preferentially concentrate LREEs relative to HREEs [11]. The presence of negative Eu anomalies in most samples further supports derivation from felsic crustal rocks, where plagioclase fractionation commonly results in Eu depletion.

Although the overall geochemical signature suggests a dominant felsic source, minor mafic contributions cannot be excluded. The presence of hornblende-bearing metagranodiorite and amphibole-rich lithologies within the Wa-Lawra Belt suggests that volcanic and mafic plutonic rocks may have contributed detrital material to the basin. Moderate concentrations of Fe_2O_3, MgO, Cr, V, and Ni in some gneiss samples indicate limited input from mafic volcanic or volcaniclastic sources. Such mixed felsic-mafic provenance is consistent with the geological framework of the Paleoproterozoic Birimian terranes, which comprise intercalated volcanic, volcaniclastic, and sedimentary successions intruded by granitoids [16,17].

Several geochemical indicators further constrain the provenance of the graphite-bearing rocks. The strong enrichment of LREEs over HREEs, together with negative Eu anomalies, is consistent with derivation from weathered felsic rocks of the upper continental crust [11]. The relatively flat HREE patterns and low concentrations of compatible elements such as Cr and Ni in most samples suggest limited contribution from ultramafic or primitive mafic sources.

The trace-element spider diagrams are characterized by enrichment in Th, Rb, K, and Ba relative to Nb and Ti. High Th/Nb and LILE/HFSE ratios are commonly associated with sediments derived from continental crustal sources and are widely used as indicators of felsic provenance [12]. Similarly, the pronounced negative Nb and Ti anomalies displayed by the graphite schists and gneisses are typical of sediments derived from evolved continental arc and granitoid sources.

The relatively high ΣREE concentrations observed in several graphite schist and gneiss samples also support derivation from felsic source rocks. Granitic and granodioritic rocks generally contain higher total REE abundances than mafic rocks and produce sedimentary deposits enriched in LREEs [11,52]. The moderate to strong REE fractionation observed in the studied rocks therefore reflects inheritance from compositionally evolved continental crust.

Petrographic evidence is also consistent with a predominantly felsic source. The abundance of quartz-rich lithologies, the presence of feldspar-derived mineral assemblages, and the occurrence of muscovite-rich graphite schists suggest derivation from mature siliciclastic sediments deposited in a tectonically stable continental environment. The original sediments likely consisted of quartz-rich clastic material interlayered with organic-rich pelitic horizons that later underwent regional metamorphism and graphitization.

In all, the petrographic, trace-element, and REE data indicate that the protoliths of the Kambale graphite-bearing rocks were derived mainly from felsic continental crust, probably involving erosion of Birimian granitoids and felsic volcanic rocks, with minor contributions from associated mafic volcanic units. This provenance interpretation is consistent with sediment accumulation within a Paleoproterozoic continental-margin to continental-arc basin prior to subsequent burial, metamorphism, and graphite mineralization.

5.4.2. Geochemical Characteristics of Graphite Schists

The geochemical characteristics of the graphite schists provide important constraints on the composition of their sedimentary precursors and the depositional environment in which they accumulated. Their relatively high SiO_2 and Al_2O_3 contents, coupled with low MgO and TiO_2 concentrations, indicate that the sediments were derived predominantly from felsic continental crust [11,12]. This interpretation is supported by trace-element systematics and REE distributions characterized by enrichment of LREEs relative to HREEs, together with pronounced negative Nb-Ta-Ti anomalies. Such geochemical signatures are typical of sediments sourced from evolved continental crust and granitoid terranes and are widely reported from felsic-derived sedimentary sequences [11,53].

Although the overall geochemical signature is dominantly felsic, moderate concentrations of compatible elements such as Cr, V, and Ni indicate that minor contributions from mafic volcanic or volcaniclastic rocks were also present. This mixed felsic-mafic provenance is consistent with the geological setting of the Paleoproterozoic Birimian terranes, where sedimentary basins developed adjacent to granitoid intrusions and volcanic successions and received detritus from both lithological sources [16,17]. Consequently, the graphite schists are interpreted to have originated from siliciclastic sediments deposited in a basin influenced predominantly by felsic crustal sources but with subordinate volcanic input.

Manganese concentrations exhibit marked variability in the graphite schists, ranging from 449 to >10,000 ppm. The exceptionally high Mn concentration in ASG-2M is also reflected in its MnO concentration of 20.10 wt.% in the major-element dataset (Table 1), confirming pronounced Mn enrichment in this sample. The exceptionally high Mn concentration in ASG-2M is accompanied by elevated Cu, Zn, Ni, and Li concentrations, suggesting localized enrichment of several trace elements within this graphite-schist horizon. The occurrence of elevated Mn is also noteworthy in the historical context of the Kambale area, where the graphite deposit was reportedly identified in the 1960s by Russian geologists during prospecting for manganese [https://www.castleminerals.com/kambale]. This historical association suggests that Mn enrichment is a recognized feature of the local geological setting. The Mn enrichment may reflect a combination of sedimentary provenance and localized depositional–diagenetic processes. The moderate Cr, V, and Ni concentrations indicate a subordinate contribution from mafic volcanic or volcaniclastic material, which may have provided an additional source of Mn. In addition, variations in organic-matter accumulation and basin redox conditions during sediment deposition and early diagenesis may have influenced Mn mobility and subsequent retention [11,38]. The heterogeneous distribution of Mn therefore suggests localized chemical variability within the sedimentary basin rather than a uniformly Mn-enriched depositional environment or a separate Mn mineralization event.

The elevated total carbon contents of the graphite schists from the ore zone, reaching up to 17.29 wt.%, indicate substantial carbon enrichment inherited from the original sedimentary succession. The occurrence of carbon-rich horizons within graphite schists containing predominantly felsic-derived siliciclastic material is consistent with the deposition and preservation of organic-rich sediments within the basin prior to metamorphism. Subsequent regional metamorphism transformed the carbonaceous material into crystalline graphite while largely preserving the geochemical characteristics of the sedimentary precursor.

Overall, the geochemical evidence indicates that the graphite schists were derived predominantly from felsic continental crust with minor mafic contributions and accumulated within a chemically heterogeneous sedimentary basin. The enrichment of LREEs, negative Nb-Ta-Ti anomalies, elevated total carbon contents, and variable Mn concentrations collectively support deposition of carbon-bearing siliciclastic sediments that were subsequently

metamorphosed and graphitized during the Eburnean tectonometamorphic evolution of the Wa-Lawra Belt.

5.4.3. Tectonic Affinity and Geodynamic Setting of the Granitoid Protoliths

The Nb/Yb-Th/Yb discrimination diagrams provide insights into the tectonic affinity of the granitoid protoliths represented by the gneisses and metagranodiorite (Figure 12a,b). Most samples plot above the MORB-OIB mantle array and are characterized by elevated Th/Yb ratios relative to Nb/Yb. Such relationships indicate enrichment in crustal-derived components relative to mantle-derived magmas and suggest significant involvement of evolved continental material in magma generation [53,54]. Several gneiss samples extend towards the deep crustal recycling field, reflecting a stronger crustal imprint than that observed in the metagranodiorite.

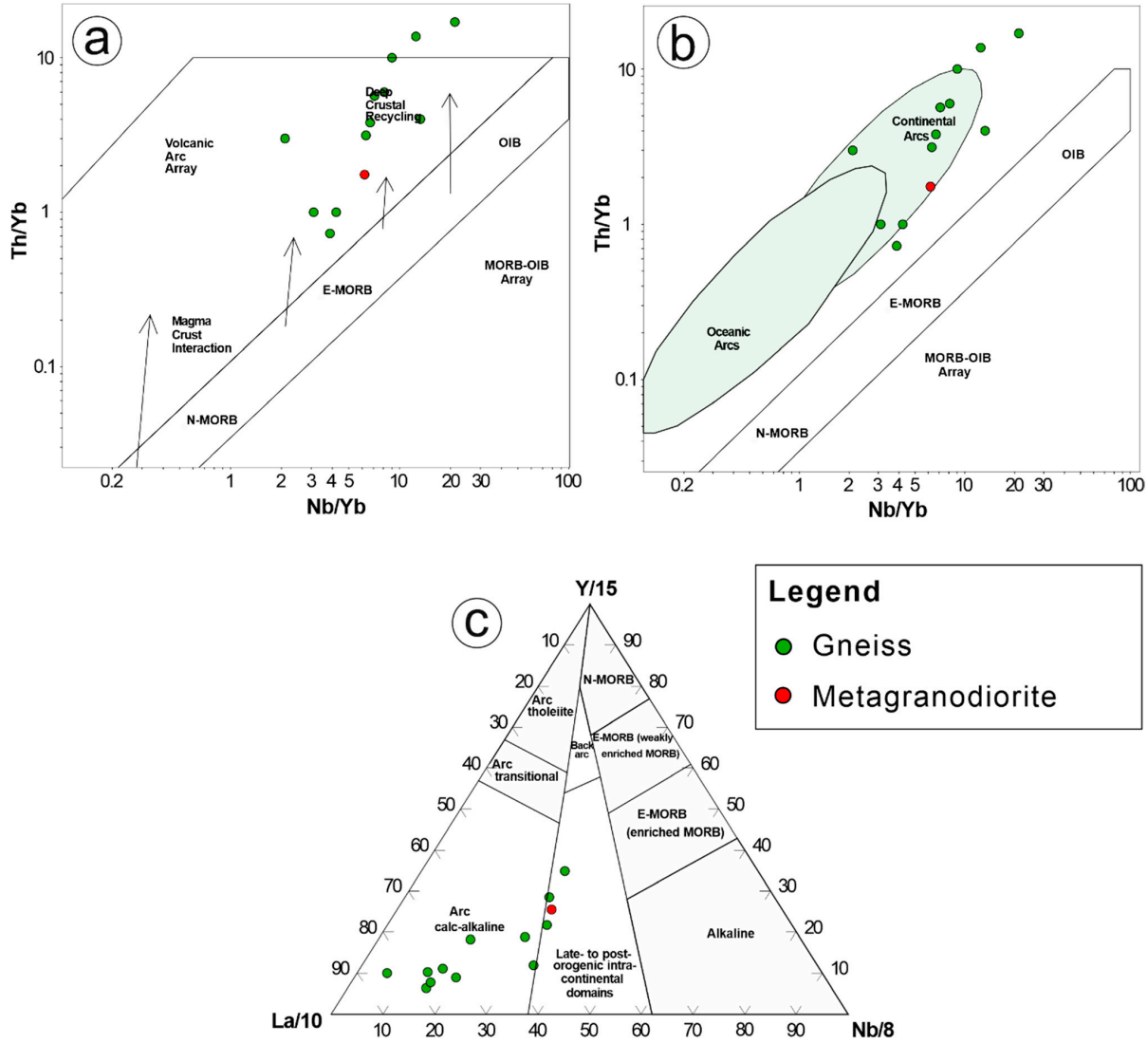


Figure 12. Tectonic discrimination diagrams for gneisses and metagranodiorite from the Kambale Graphite Deposit, Wa-Lawra Belt, Ghana: (**a**) Nb/Yb versus Th/Yb diagram showing mantle-array affinities, crustal contamination, and deep crustal recycling trends; (**b**) Nb/Yb versus Th/Yb tectonic discrimination diagram illustrating affinities with continental arc magmatic settings; and (**c**) La/10-Y/15-Nb/8 ternary diagram showing predominantly arc calc-alkaline signatures with minor late- to post-orogenic intracontinental affinities (After [54,55]).

Majority of the samples occupy the continental arc field on the tectonic discrimination diagram (Figure 12b), indicating derivation from magmas generated in a convergent-margin setting. The distribution of the samples suggests that magma evolution involved interaction between mantle-derived melts and continental crust, resulting in enrichment of Th relative to Nb and Yb. Compared with the gneisses, the metagranodiorite samples exhibit more moderate Th/Yb values, suggesting comparatively lower degrees of crustal involvement.

Additional evidence is provided by the La/10-Y/15-Nb/8 ternary diagram (Figure 12c), where most samples plot within the arc calc-alkaline field. This distribution indicates an affinity with calc-alkaline magmatic systems commonly associated with subduction-related continental margins. A small number of samples plot close to the late- to post-orogenic intracontinental field, suggesting limited late-stage crustal reworking or magmatic evolution. Collectively, the discrimination diagrams indicate that the granitoid protoliths of the gneisses and metagranodiorite were generated within a continental arc environment and subsequently underwent crustal reworking during the Paleoproterozoic evolution of the Birimian terranes.

Additional support for a convergent-margin affinity is provided by the Rb-(Y + Nb) and Nb-Y tectonic discrimination diagrams (Figure 13). Most gneiss samples plot within the Volcanic Arc Granite (VAG) and Syn-Collisional Granite (syn-COLG) fields, while the metagranodiorite falls mainly within the syn-collisional field. The predominance of VAG and syn-COLG signatures suggests that the source rocks were derived largely from granitoids generated during subduction-related magmatism and subsequent continental collision [56]. The absence of significant sample concentrations within the Ocean Ridge Granite (ORG) field and the limited influence of the Within-Plate Granite (WPG) field indicate that extensional tectonic environments played only a minor role in the generation of the source rocks. Instead, the combined tectonic discrimination diagrams consistently point to derivation from felsic to intermediate arc-related granitoids that formed in a continental margin setting affected by crustal recycling and collisional tectonics.

Thus, the tectonic discrimination diagrams indicate that the sedimentary precursors of the Kambale graphite-bearing rocks were derived predominantly from felsic to intermediate calc-alkaline rocks generated within continental arc and syn-collisional tectonic environments. These results support erosion of Birimian arc-related granitoids and felsic volcanic rocks during the Eburnean Orogeny, followed by deposition of quartz-rich and organic-rich sediments that were subsequently metamorphosed and graphitized during the tectonometamorphic evolution of the Wa-Lawra Belt.

5.4.4. Crustal Evolution and Source Characteristics of the Granitoid Protoliths

The Nb-Y-Ce and Nb-Y-3Ga discrimination diagrams (Figure 14a,b) indicate that the gneisses and metagranodiorite plot exclusively within the A_2 (lower crust) field. The concentration of samples within this field suggests derivation from evolved continental crustal sources that experienced significant crustal reworking and magmatic differentiation prior to metamorphism. In contrast, none of the samples plot within the mantle-dominated A_1 field, indicating limited direct contribution from juvenile mantle-derived magmas. Such compositional characteristics are typical of felsic granitoids generated through melting and reworking of pre-existing continental crust [57,58].

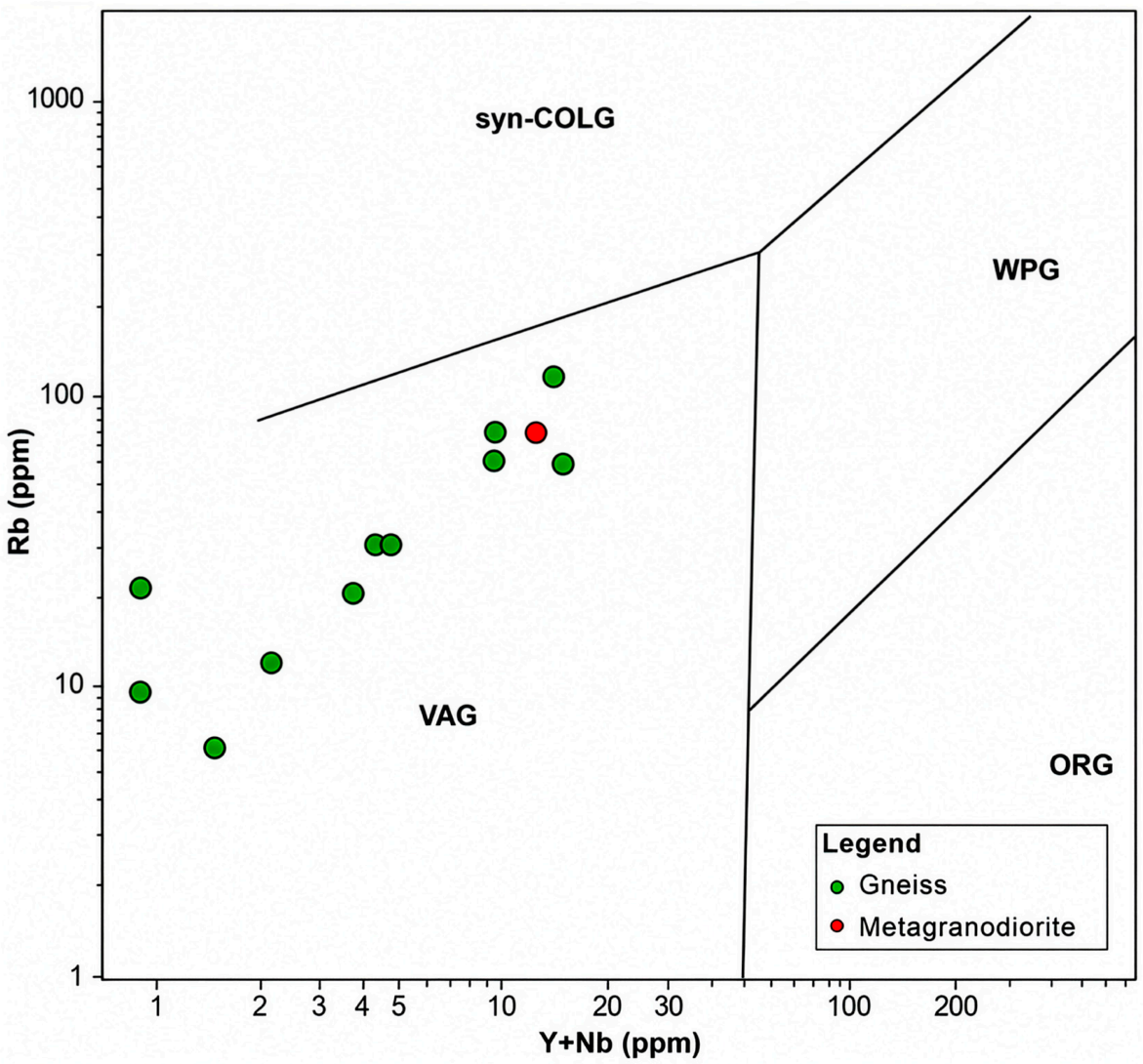


Figure 13. Rb versus (Y + Nb) tectonic discrimination diagram for the gneisses and metagranodiorite of the Kambale Graphite Deposit, Wa-Lawra Belt, Ghana. Fields after [56] are used to evaluate the tectonic affinity of the granitoid protoliths represented by the metamorphosed granitoid rocks.

The Rb/Nb versus Y/Nb diagram (Figure 14c) provides further evidence for a crustal origin of the granitoid protoliths. Most gneiss and metagranodiorite samples cluster within, or immediately adjacent to, the A_2 field and are characterized by moderate to high Rb/Nb ratios. These geochemical features are consistent with evolved felsic rocks that have undergone prolonged crustal differentiation and recycling processes [57]. The distribution of the samples suggests that their precursor magmas were derived predominantly from reworked continental crust rather than juvenile mantle sources.

The lower-crustal affinity identified in all three discrimination diagrams is consistent with the petrographic evidence for granitoid protoliths and with the granitic to granodioritic compositions indicated by the major-element classification diagrams (Figure 14a–c). Together, these observations suggest that the gneisses represent orthogneisses derived from felsic granitoid precursors, whereas the metagranodiorite represents less deformed equivalents of related granitoid rocks. The geochemical signatures therefore reflect extensive crustal reworking during the Paleoproterozoic evolution of the Birimian terranes and support derivation from compositionally evolved continental crustal sources.

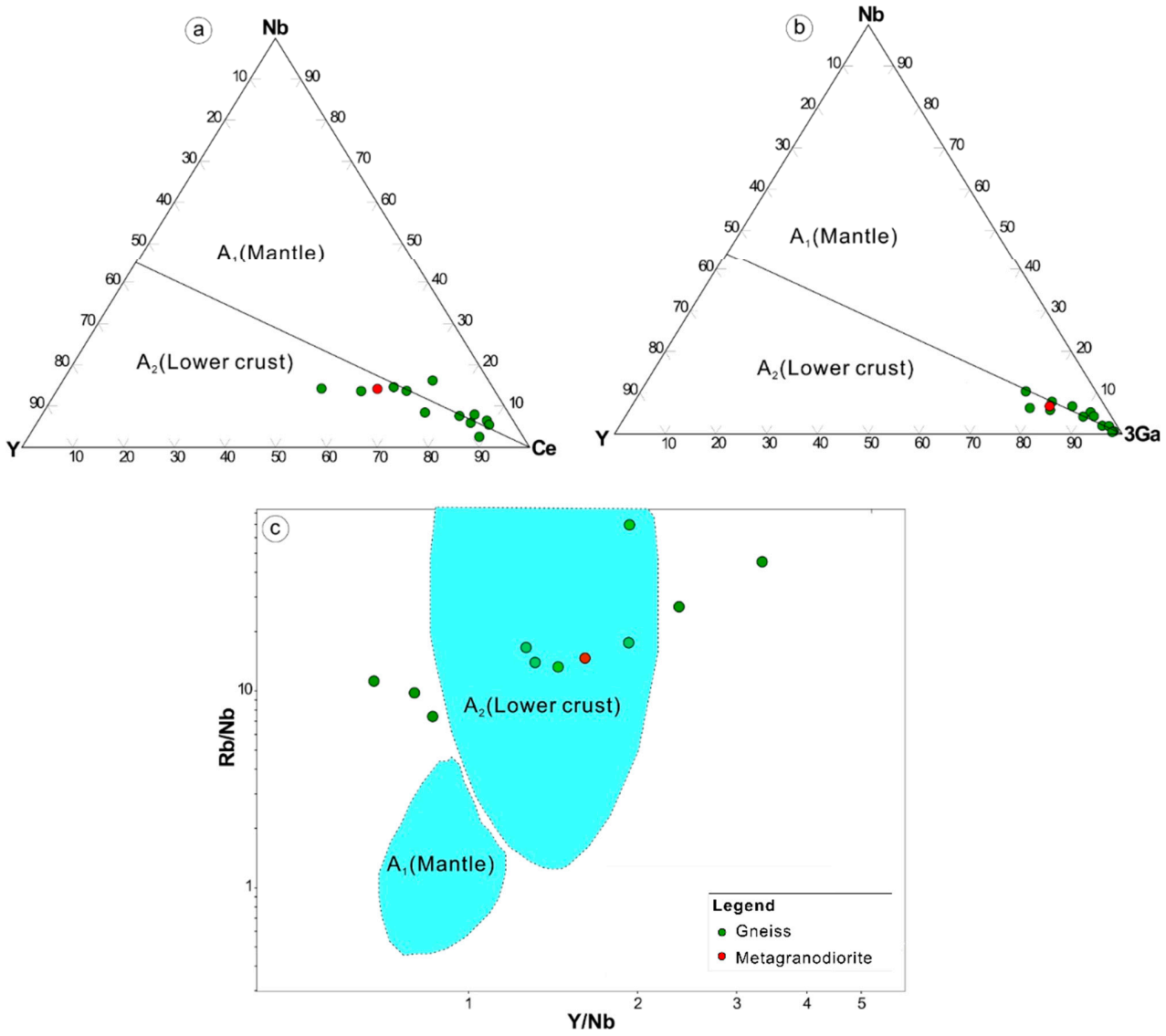


Figure 14. Source discrimination diagrams for gneisses and metagranodiorite from the Kambale Graphite Deposit, Wa-Lawra Belt, Ghana: (**a**) Nb-Y-Ce ternary diagram; (**b**) Nb-Y-3Ga ternary diagram; and (**c**) Rb/Nb versus Y/Nb diagram. The diagrams indicate that the studied rocks plot predominantly within the A_2 (Lower Crust) field, suggesting derivation from reworked continental crust with limited mantle contribution. Diagrams after Eby [57].

5.5. Carbon Isotope Constraints on the Origin of Graphite Mineralization

Carbon isotope compositions of the graphite-bearing carbonaceous material in the graphite schists provide an important constraint on the source of carbon and on the processes involved in graphite mineralization. The $\delta^{13}C$ values of carbonaceous material associated with graphite deposits can be broadly compared with three major carbon reservoirs: (1) biogenic or organic carbon, which typically exhibits strongly negative $\delta^{13}C$ values between approximately −40‰ and −10‰; (2) mantle-derived carbon, which commonly ranges from about −10‰ to −5‰; and (3) carbonate-derived carbon, which generally displays values between −5‰ and +5‰ [8,41,51,59].

Figure 15 compares the carbon isotopic composition of graphite schists from the Kambale deposit with graphite occurrences from other parts of the world. The graphite schists in Kambale exhibit $\delta^{13}C$ values ranging from approximately −31‰ to −24‰. All analyzed samples therefore plot entirely within the biogenic carbon field, far removed from the mantle and carbonate carbon reservoirs.

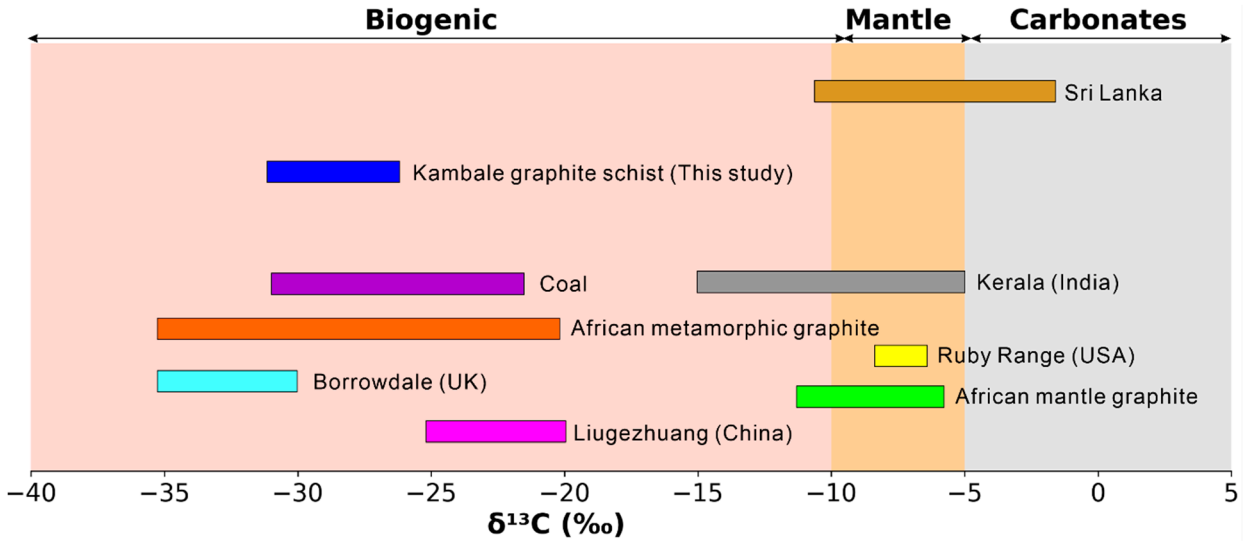


Figure 15. Comparison of $\delta^{13}C$ values of graphite schists from the Kambale Graphite Deposit with selected graphite deposits and carbon reservoirs worldwide. All Kambale samples plot within the biogenic carbon field, indicating an organic sedimentary origin for the graphite. Fields after Hoefs and Frey [8], Luque et al. [45], Deines [60], Buseck and Beyssac [41], Satish-Kumar [51], Case et al. [10], and Liu et al. [13].

The strongly negative $\delta^{13}C$ values indicate that the carbon preserved in the Kambale graphite-bearing rocks was originally derived predominantly from organic matter that accumulated within sedimentary environments prior to metamorphism. Such isotopic signatures are consistent with carbon fixed through biological processes, where photosynthetic fractionation preferentially enriches organic matter in the lighter isotope, ^{12}C, resulting in negative $\delta^{13}C$ values [8,41]. During subsequent burial and metamorphism, this organic-rich carbonaceous material was progressively transformed and structurally ordered, ultimately producing crystalline graphite.

The isotopic compositions obtained from Kambale are comparable to those reported for other metamorphic graphite deposits worldwide. The values overlap closely with the ranges reported for African metamorphic graphite deposits, the Borrowdale graphite deposit in the United Kingdom, and the Liugezhuang graphite deposit in China (Figure 15). Similar $\delta^{13}C$ signatures have been interpreted as evidence for graphitization of organic-rich sedimentary protoliths during regional metamorphism [4,10,45]. Furthermore, the Kambale values overlap those reported for coal-derived carbonaceous materials, supporting derivation from originally organic-rich sediments.

In contrast, the Kambale samples show no overlap with the mantle carbon field represented by African mantle graphite and the Ruby Range graphite occurrence. Mantle-derived carbon is generally characterized by less negative $\delta^{13}C$ values and typically reflects carbon introduced through magmatic or deep-seated mantle processes [51,59,60]. Likewise, none of the Kambale samples approach the carbonate field, indicating that decarbonation of carbonate rocks was not the primary source of carbon responsible for the graphite mineralization.

The isotopic data therefore supports the petrographic and mineralogical evidence indicating that the graphite formed through metamorphic transformation of organic-rich sedimentary material. The preservation of strongly negative $\delta^{13}C$ values despite amphibolite-facies metamorphism suggests limited isotopic modification during graphitization. Experimental and natural studies have demonstrated that although metamorphism increases the crystallinity and ordering of carbonaceous matter, it generally produces

only minor changes in carbon isotopic composition unless extensive fluid-rock interaction occurs [7,10,41].

Carbon isotope data provide strong evidence that the Kambale Graphite Deposit formed through the graphitization of biogenic organic matter originally deposited in sedimentary rocks and subsequently subjected to amphibolite-facies metamorphism during the Paleoproterozoic evolution of the Wa-Lawra Belt. Uniformly negative $\delta^{13}C$ values, together with petrographic, geochemical, and tectonic evidence, support a genetic model involving deposition of organic-rich sediments in a continental arc basin, burial and preservation of organic matter, and progressive metamorphic recrystallization into crystalline flake graphite [4,10,13].

5.6. Proposed Tectonic Evolution Model for the Kambale Graphite Deposit

The integrated petrographic, SEM-BSE/EDX, geochemical, and carbon isotope data suggest that the Kambale Graphite Deposit formed through the metamorphic transformation of carbonaceous sediments deposited within the Paleoproterozoic Wa-Lawra Belt and subsequently modified during Eburnean tectonometamorphic events. The proposed evolutionary model involves sedimentation, regional metamorphism, graphitization, deformation-assisted recrystallization, and post-metamorphic uplift and preservation (Figure 16).

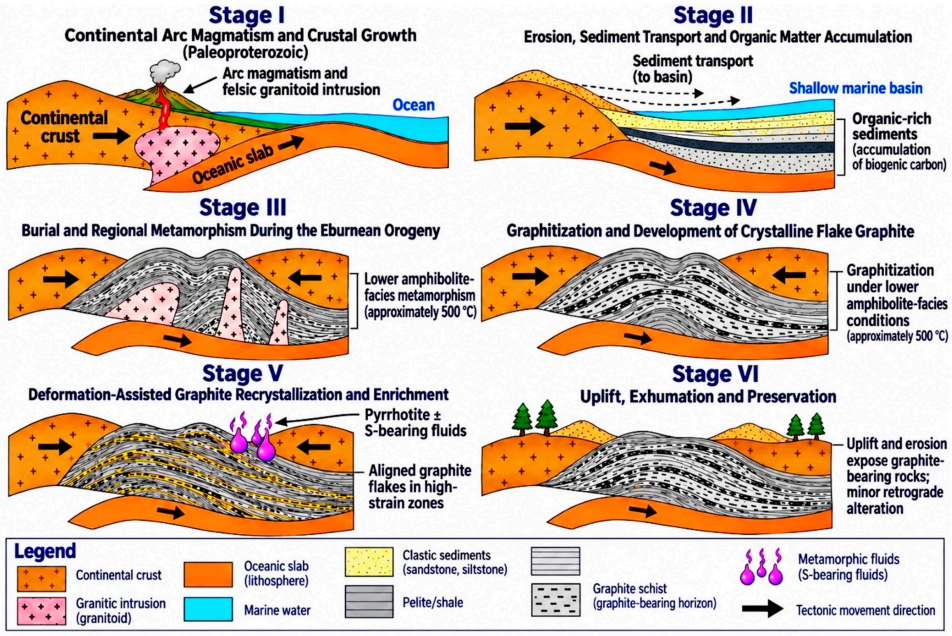


Figure 16. Proposed tectonic evolution model for the Kambale Graphite Deposit. The model illustrates the six major stages of graphite deposit formation in the Wa-Lawra Belt, Ghana: (I) continental arc magmatism and crustal growth in a Paleoproterozoic convergent-margin setting; (II) erosion of arc-related rocks, sediment transport, and deposition of organic-rich sediments in a reducing basin; (III) burial and amphibolite-facies metamorphism during the Eburnean Orogeny; (IV) graphitization of biogenic organic matter to form crystalline flake graphite under lower amphibolite-facies conditions; (V) deformation-assisted graphite recrystallization, grain coarsening, and redistribution associated with regional metamorphism and shearing; and (VI) post-orogenic uplift, exhumation, and preservation of the graphite-bearing schists. The model is constrained by integrated petrographic, SEM-EDX, whole-rock geochemical, carbon isotope, provenance, and tectonic discrimination data from the Kambale Graphite Deposit.

Stage I: Deposition of Carbonaceous Sediments—The precursor to the graphite mineralization is interpreted to have been a sedimentary sequence composed of quartz-rich siliciclastic sediments interlayered with organic-rich pelitic horizons. Carbon isotope com-

positions, together with the abundance of graphite within metasedimentary units, are consistent with the accumulation and preservation of organic matter prior to metamorphism. Sedimentation occurred during the Paleoproterozoic evolution of the Birimian terrane, when active crustal growth and basin development accompanied subduction-related magmatism and continental arc evolution [11,12,54].

Stage II: Regional Metamorphism During the Eburnean Orogeny—Progressive burial, crustal shortening, and crustal thickening during the Eburnean Orogeny subjected the sedimentary succession to regional metamorphism. Mineral assemblages comprising quartz, muscovite, biotite, hornblende, plagioclase, and K-feldspar, indicate metamorphic conditions corresponding predominantly to the lower amphibolite facies (approximately 500–600 °C). During this stage, the original carbonaceous sediments were transformed into graphite schists, while associated granitoid bodies underwent deformation and metamorphic recrystallization to form orthogneisses and metagranodiorite.

Stage III: Graphitization and Development of Crystalline Flake Graphite—Increasing metamorphic temperatures promoted progressive transformation of sedimentary organic carbon into crystalline graphite. Graphite occurs predominantly as fine crystalline flakes, with locally coarser flakes intimately associated with recrystallized quartz and muscovite and aligned parallel to the dominant foliation. Such textures are characteristic of graphitization during medium- to high-grade regional metamorphism and reflect increasing structural ordering of carbonaceous material [7,41]. The development of locally coarser, well-crystallized graphite flakes is consistent with progressive graphitization and grain coarsening under lower amphibolite-facies metamorphic conditions. Carbon isotope compositions ranging from approximately −31.83‰ to −24.33‰ (VPDB) are consistent with an organic carbon precursor and strongly support derivation from sedimentary organic matter rather than mantle-derived carbon sources [8,10,41].

Stage IV: Deformation-Assisted Recrystallization and Graphite Concentration—Regional deformation accompanying metamorphism played an important role in graphite recrystallization and concentration. The preferred orientation of graphite flakes parallel to schistosity, together with dynamically recrystallized quartz and well-developed lepidoblastic textures, indicates syn-tectonic graphite growth. SEM-BSE observations show that graphite commonly occurs along foliation planes, grain boundaries, and interstitial domains between quartz and muscovite, consistent with deformation-assisted graphite coarsening and redistribution during progressive metamorphism [10,33,51]. These processes contributed to the development of economically significant graphite-rich horizons within the graphite schists.

Stage V: Sulfide Development and Metamorphic Re-equilibration—Pyrrhotite occurs as locally disseminated coarse grains intimately associated with graphite, quartz, and muscovite. Textural relationships observed in SEM-BSE images indicate that sulfides formed or recrystallized during metamorphism and became incorporated into the graphite-bearing assemblage during mineral re-equilibration. The close association between graphite and pyrrhotite suggests that both phases shared a common metamorphic history.

Stage VI: Exhumation and Preservation—Following peak metamorphism, uplift and erosion exposed the graphite-bearing sequence. Evidence for retrograde alteration is limited and is represented mainly by epidote growth and minor feldspar alteration. The preservation of crystalline flake graphite, strong schistosity, and amphibolite-facies mineral assemblages indicates that post-peak modification was relatively minor and did not significantly overprint the graphite mineralization. Consequently, the primary metamorphic and deformational features responsible for graphite formation and concentration remain well preserved within the Kambale deposit.

In summary, the Kambale deposit is interpreted as a metamorphic flake graphite occurrence formed through graphitization of organic-rich sediments during regional amphibolite-facies metamorphism and subsequently enhanced by deformation-assisted recrystallization during the Eburnean tectonometamorphic evolution of the Wa-Lawra Belt [7,10,33,41,50]. This model is consistent with the mineralogical, isotopic, and textural characteristics of the deposit and with the broader geological evolution of the Paleoproterozoic Birimian terranes of northwestern Ghana.

6. Conclusions

This study aimed to characterize the petrographic and mineralogical features of the graphite-bearing rocks at the Kambale Graphite Deposit, constrain the provenance and depositional conditions of their protoliths using whole-rock geochemistry, determine the source of carbon using stable carbon isotope compositions, and develop an integrated genetic model for graphite mineralization within the Eburnean tectono-metamorphic evolution of the Paleoproterozoic Wa–Lawra Belt. The principal findings are summarized as follows:

- The Kambale Graphite Deposit represents a metamorphic flake-graphite system formed through the graphitization of carbonaceous sedimentary precursors during regional Eburnean metamorphism and deformation.
- Graphite occurs predominantly as fine crystalline flakes closely associated with quartz, muscovite, and minor pyrrhotite and preferentially aligned parallel to the dominant foliation, reflecting syn-metamorphic recrystallization, deformation-assisted redistribution, and local coarsening.
- The stable carbon isotope compositions of the graphite-bearing carbonaceous material in the graphite schists ($\delta^{13}C$ = −31.83‰ to −24.33‰ VPDB) strongly support an organic-derived carbon source and are consistent with graphitization of carbonaceous sedimentary precursors.
- The mineralogical and textural characteristics indicate predominantly lower amphibolite-facies metamorphic recrystallization.
- The associated gneisses and metagranodiorite are interpreted as granitoid-derived meta-igneous rocks with granitic to granodioritic protolith affinities and predominantly peraluminous compositions, indicating significant involvement of evolved continental crust and a continental-arc setting.
- The whole-rock trace-element and REE characteristics indicate that the sedimentary precursors of the graphite-bearing rocks were derived predominantly from felsic continental crust with subordinate mafic input and were subsequently metamorphosed and graphitized during the Eburnean tectono-metamorphic evolution of the Wa–Lawra Belt.
- The integrated petrographic, SEM-BSE/EDX, geochemical, and stable carbon isotope evidence supports a genetic sequence involving deposition of carbonaceous sediments, regional metamorphism and graphitization, deformation-assisted graphite recrystallization and local coarsening, minor pyrrhotite formation, and subsequent preservation of the graphite-bearing sequence.
- The proposed genetic model is constrained by the absence of direct geochronological and quantitative thermobarometric data, and therefore the precise P–T conditions and timing of metamorphism and graphite mineralization at Kambale remain to be established.

Supplementary Materials: The following supporting information can be downloaded at: https://www.mdpi.com/article/10.3390/min16101060/s1, Table S1: Bureau Veritas Commodities Canada Ltd. Laboratory Analytical Data and Quality-Control Results for the Kambale Graphite Deposit, Ghana; Table S2: Cornell University Stable Isotope Laboratory Analytical Data and Quality-Control Results for Graphite Schists from the Kambale Graphite Deposit, Ghana.

Author Contributions: Conceptualization, E.D.S.; methodology, E.D.S. and E.B.F.; software, E.D.S., M.A.G. and S.E.K.T.; validation, E.D.S., E.B.F., M.A.G., Y.D., J.N.A., S.J.A. and A.L.; formal analysis, E.D.S., E.B.F., A.N.G. and B.M.; investigation, E.D.S., E.B.F., A.N.G. and B.M.; resources, E.D.S.; data curation, E.D.S., E.B.F., M.A.G., Y.D., J.N.A., A.N.G., B.M., S.J.A. and A.L.; writing—original draft preparation, E.D.S. and J.N.A.; writing—review and editing, E.D.S., E.B.F., M.A.G., Y.D., S.J.A. and A.L.; visualization, E.D.S., J.N.A. and S.E.K.T.; supervision, E.D.S. and E.B.F.; project administration, E.D.S.; funding acquisition, E.D.S. All authors have read and agreed to the published version of the manuscript.

Funding: This research was financially supported by the Ghana Chamber of Mines' Tertiary Education Fund (GCM-TEF) Faculty Members Research Grant (Award Reference No. 118/U.9/24L).

Data Availability Statement: The original contributions presented in this study are included in the article. Further inquiries can be directed to the corresponding author.

Acknowledgments: The authors gratefully acknowledge the financial support provided by the Ghana Chamber of Mines' Tertiary Education Fund (GCM-TEF) through the Faculty Members Research Grant (Award Reference No. 118/U.9/24L). This support facilitated the field investigations, laboratory analyses, and data interpretation presented in this study. The authors sincerely thank Kimberlee L. Sparks of the Cornell University Stable Isotope Laboratory for conducting the carbon isotope analyses. The authors also acknowledge the University of Mines and Technology (UMaT), Tarkwa, for institutional support and access to facilities that contributed to the successful completion of this work. Appreciation is further extended to all individuals and organizations who provided logistical, technical, and field assistance throughout the study.

Conflicts of Interest: Samuel Edem Kodzo Tetteh is an employee of Onyx Gold Corp. The research presented in this manuscript was conducted independently and did not receive funding or financial support from Onyx Gold Corp. The paper reflects the views of the authors and not necessarily those of the company. The authors declare no other conflicts of interest.

Abbreviations

The following abbreviations are used in this manuscript:

A/CNK	Alumina saturation index: $Al_2O_3/(CaO + Na_2O + K_2O)$
A/NK	Alumina saturation index: $Al_2O_3/(Na_2O + K_2O)$
BSE	Backscattered electron
Ce/Ce*	Cerium anomaly
EDX	Energy-dispersive X-ray spectroscopy
Eu/Eu*	Europium anomaly
HFSE	High-field-strength elements
HREE	Heavy rare earth elements
IAEA	International Atomic Energy Agency
ICP-ES	Inductively coupled plasma emission spectrometry
ICP-MS	Inductively coupled plasma mass spectrometry
LILE	Large-ion lithophile elements
LOI	Loss on ignition
LREE	Light rare earth elements
MORB	Mid-ocean ridge basalt
OIB	Ocean island basalt
PPL	Plane-polarized light
QA/QC	Quality assurance/quality control
REE	Rare earth element
SEM	Scanning electron microscopy
SEM-EDS	Scanning electron microscopy–energy-dispersive spectroscopy
TAS	Total alkali–silica
V-PDB	Vienna Pee Dee Belemnite
XPL	Cross-polarized light

References

1. Asenbauer, J.; Eisenmann, T.; Kuenzel, M.; Kazzazi, A.; Chen, Z.; Bresser, D. The success story of graphite as a lithium-ion anode material—Fundamentals, remaining challenges, and recent developments including silicon (oxide) composites. *Sustain. Energy Fuels* **2020**, *4*, 5387–5416. [CrossRef]
2. Robinson, G.R., Jr.; Hammarstrom, J.M.; Olson, D.W. Graphite. In *Critical Mineral Resources of the United States—Economic and Environmental Geology and Prospects for Future Supply*; Schulz, K.J., DeYoung, J.H., Jr., Seal, R.R., II, Bradley, D.C., Eds.; Professional Paper; United States Geological Survey: Reston, VA, USA, 2017. [CrossRef]
3. Zhao, H.; Zuo, H.; Wang, J.; Jiao, S. Practical application of graphite in lithium-ion batteries: Modification, composite, and sustainable recycling. *J. Energy Storage* **2024**, *98*, 113125. [CrossRef]
4. Wang, J.Y.; Liu, J.C.; Zhang, H.D.; Zhang, H.R.; Li, Y. Metamorphism, geochemistry, and carbon source on sedimentary-metamorphic graphite deposits in eastern Shandong, China. *Geol. J.* **2019**, *55*, 3748–3769. [CrossRef]
5. Santoro, L.; Bertone, V.; Ferrando, S.; Groppo, C. New insights into graphite deposits in Chisone and Germanasca Valleys (Dora-Maira Massif, Western Italian Alps): Scientific advances and applied perspectives. *Minerals* **2025**, *15*, 455. [CrossRef]
6. Hegeman, P.; Zhou, L. Towards a sustainable supply of graphite: A geological way forward. *Earth Sci. Syst. Soc.* **2025**, *5*, esss2024-014. [CrossRef]
7. Landis, C.A. Graphitization of dispersed carbonaceous material in metamorphic rocks. *Contrib. Mineral. Petrol.* **1971**, *30*, 34–45. [CrossRef]
8. Hoefs, J.; Frey, M. The isotopic composition of carbonaceous matter in a metamorphic profile from the Swiss Alps. *Geochim. Cosmochim. Acta* **1976**, *40*, 945–951. [CrossRef]
9. Wilde, S. Geological setting and controls on the development of graphite, sillimanite and phosphate mineralization within the Jiamusi Massif: An exotic fragment of Gondwanaland located in north-eastern China? *Gondwana Res.* **1999**, *2*, 21–46. [CrossRef]
10. Case, G.N.D.; Karl, S.M.; Regan, S.P.; Johnson, C.A.; Ellison, E.T.; Caine, J.S.; Holm-Denoma, C.S.; Pianowski, L.S.; Marsh, J.H. Insights into the metamorphic history and origin of flake graphite mineralization at the graphite Creek graphite deposit, Seward Peninsula, Alaska, USA. *Miner. Depos.* **2023**, *58*, 939–962. [CrossRef]
11. Taylor, S.R.; McLennan, S.M. *The Continental Crust: Its Composition and Evolution*; Blackwell Scientific Publications: Oxford, UK, 1985; Available online: https://commons.library.stonybrook.edu/geo-articles/12/ (accessed on 26 August 2026).
12. Bhatia, M.R.; Crook, K.A.W. Trace element characteristics of graywackes and tectonic setting discrimination of sedimentary basins. *Contrib. Mineral. Petrol.* **1986**, *92*, 181–193. [CrossRef]
13. Liu, F.; Rao, W.; Zhang, Y.; Yao, W.; Shi, L.; Xu, M.; Ren, S.; Li, X.; Li, Z. Geochemical characteristics of the Shuanghu crystalline graphite deposit in East China: Implications for original rocks, sedimentary environments and carbon sources. *Front. Earth Sci.* **2025**, *13*, 1576709. [CrossRef]
14. Liang, Y.; Yuan, W.; Liu, J.; Nechaev, V.P.; Moore, T.A.; Zhang, S.; Wang, Q.; Zheng, J.; Yan, X.; Yao, M.; et al. Biomarkers and organic carbon isotopes in Pennsylvanian–Early Permian coals of the Ordos Basin: Implications for palaeoenvironmental evolution in North China. *Palaeogeogr. Palaeoclimatol. Palaeoecol.* **2025**, *680*, 113369. [CrossRef]
15. Li, K.; Lu, H.; He, X.-F.; Xu, Z.; Liu, Q. Petrographic and carbon isotopic evidence for the sources and evolution of natural coal-derived graphite in Lutang area, South China. *Int. J. Coal Geol.* **2026**, *321*, 105027. [CrossRef]
16. Taylor, P.N.; Moorbath, S.; Leube, A.; Hirdes, W. Early Proterozoic crustal evolution in the birimian of Ghana: Constraints from geochronology and isotope geochemistry. *Precambrian Res.* **1992**, *56*, 97–111. [CrossRef]
17. Oberthür, T. Age constraints on gold mineralization and Paleoproterozoic crustal evolution in the Ashanti belt of southern Ghana. *Precambrian Res.* **1998**, *89*, 129–143. [CrossRef]
18. Lompo, M. Paleoproterozoic structural evolution of the Man-Leo Shield (West Africa). Key structures for vertical to transcurrent tectonics. *J. Afr. Earth Sci.* **2010**, *58*, 19–36. [CrossRef]
19. Sunkari, E.D.; Zango, M.S. Preliminary investigation of the geologic controls of graphite mineralization and exploration potential of the Wa-Lawra Belt: Implications for Kambale graphite deposit. *Environ. Earth Sci.* **2018**, *8*, 77–89.
20. Sunkari, E.D.; Senne, D.; Asamoah-Boadu, G.; Fiadonu, E.B.; Yılmaz Demir, Y.; Adams, S.J. Lithological and mineralogical characteristics of graphite ore from the Kambale graphite deposit in the Wa-Lawra belt, Ghana: Implications from petrography and scanning electron microscopic studies. In Proceedings of the VI International Turkic World Congress on Science and Engineering (TURK-COSE 2024), Baku, Azerbaijan, 19–21 December 2024; Available online: https://turk-cose.ohu.edu.tr/docs/bookofproceedings2024.pdf (accessed on 19 September 2026).
21. Agyei-Duodu, J.; Loh, G.K.; Boamah, K.O.; Baba, M.; Hirdes, W.; Toloczyki, M.; Davis, D.W. *Geological Map of Ghana 1:1000000*; Geological Survey Department of Ghana (GSD) Report; GSD: Accra, Ghana, 2009; Volume 1. Available online: https://www.scirp.org/reference/referencespapers?referenceid=2539793 (accessed on 26 August 2026).
22. Amponsah, P.O.; Salvi, S.; Didier, B.; Baratoux, L.; Siebenaller, L.; Jessell, M.; Nude, P.M.; Gyawu, E.A. Multistage gold mineralization in the Wa-Lawra greenstone belt, NW Ghana: The Bepkong deposit. *J. Afr. Earth Sci.* **2016**, *120*, 220–237. [CrossRef]

23. Sunkari, E.D.; Lermi, A.; Adomako-Ansah, K.; Fiadonu, E.B.; Tetteh, S.E.K.; Oppong, O.; Adams, S.J.; Demir, Y.; Ali, S. Chapter 1: Geology and Gold Mineralization Styles in Ghana. In *Geology and Gold Mineralization in Ghana: Geological Provinces and Gold Mineralization*; Sunkari, E.D., Ali, S., Eds.; Springer Nature: Cham, Switzerland, 2025; pp. 3–49. [CrossRef]
24. Perrouty, S.; Aillères, L.; Jessell, M.W.; Baratoux, L.; Bourassa, Y.; Crawford, B. Revised Eburnean geodynamic evolution of the gold-rich southern Ashanti Belt, Ghana, with new field and geophysical evidence of pre-Tarkwaian deformations. *Precambrian Res.* **2012**, *204–205*, 12–39. [CrossRef]
25. Chardon, D.; Bamba, O.; Traoré, K. Eburnean deformation pattern of Burkina Faso and the tectonic significance of shear zones in the West African Craton. *BSGF—Earth Sci. Bull.* **2020**, *191*, 2. [CrossRef]
26. Arhin, E.; Nude, P.M. Significance of regolith mapping and its implication for gold exploration in northern Ghana: A case study at Tinga and Kunche. *Geochem. Explor. Environ. Anal.* **2009**, *9*, 63–69. [CrossRef]
27. Baratoux, L.; Metelka, V.; Naba, S.; Jessell, M.W.; Grégoire, M.; Ganne, J. Juvenile Paleoproterozoic crust evolution during the Eburnean orogeny (~2.2–2.0 Ga), western Burkina Faso. *Precambrian Res.* **2011**, *191*, 18–45. [CrossRef]
28. Whitney, D.L.; Evans, B.W. Abbreviations for names of rock-forming minerals. *Am. Mineral.* **2010**, *95*, 185–187. [CrossRef]
29. Sun, S.; McDonough, W.F. Chemical and isotopic systematics of oceanic basalts: Implications for mantle composition and processes. *Geol. Soc. Lond. Spec. Publ.* **1989**, *42*, 313–345. [CrossRef]
30. Maniar, P.D.; Piccoli, P.M. Tectonic discrimination of granitoids. *Geol. Soc. Am. Bull.* **1989**, *101*, 635–643. [CrossRef]
31. Case, G.N.D. A time-space model of graphite mineral systems. *Mineral. Depos.* **2025**, *61*, 783–810. [CrossRef]
32. Luque, F.J.; Huizenga, J.M.; Crespo-Feo, E.; Wada, H.; Ortega, L.; Barrenechea, J.F. Vein graphite deposits: Geological settings, origin, and economic significance. *Mineral. Depos.* **2014**, *49*, 261–277. [CrossRef]
33. Crespo, E.; Luque, J.; Barrenechea, J.F.; Rodas, M. Mechanical graphite transport in fault zones and the formation of graphite veins. *Mineral. Mag.* **2005**, *69*, 463–470. [CrossRef]
34. Sunkari, E.D.; Kore, B.M.; Tetteh, S.E.K. Petrography and structural features of the Precambrian basement rocks in the Benin-Nigerian Shield, NW Nigeria: Implications for their correlation with South Atlantic Precambrian terranes. *AIMS Geosci.* **2022**, *8*, 503–524. [CrossRef]
35. Passchier, C.W.; Trouw, R.A.J. *Microtectonics*, 2nd ed.; Springer: Berlin/Heidelberg, Germany, 2005. [CrossRef]
36. Vernon, R.H. *A Practical Guide to Rock Microstructure*; Cambridge University Press: New York, NY, USA, 2004. [CrossRef]
37. Sunkari, E.D.; Lermi, A. Geological, mineralogical, geochemical, and petrogenetic characteristics of plutonic rocks in Çiftehan (Ulukışla-Niğde) area, south-central Türkiye: Implication for genetic link with Fe-Zn skarn mineralization. *Minerals* **2025**, *15*, 578. [CrossRef]
38. Winter, J.D. *Principles of Igneous and Metamorphic Petrology*, 2nd ed.; Pearson Education Limited: Boston, MA, USA, 2013.
39. Spear, F.S.; Pattison, D.R.M. The implications of overstepping for metamorphic assemblage diagrams (MADs). *Chem. Geol.* **2017**, *457*, 38–46. [CrossRef]
40. Bucher, K.; Grapes, R.H. *Petrogenesis of Metamorphic Rocks*, 8th ed.; Springer: Berlin/Heidelberg, Germany, 2011. [CrossRef]
41. Buseck, P.R.; Beyssac, O. From organic matter to graphite: Graphitization. *Elements* **2014**, *10*, 421–426. [CrossRef]
42. Craig, J.R.; Vokes, F.M. The metamorphism of pyrite and pyritic ores: An overview. *Mineral. Mag.* **1993**, *57*, 3–18. [CrossRef]
43. Vokes, F.M.; Craig, J.R. Post-recrystallisation mobilisation phenomena in metamorphosed stratabound sulphide ores. *Mineral. Mag.* **1993**, *57*, 19–28. [CrossRef]
44. Hall, A.J. Pyrite-pyrrhotine redox reactions in nature. *Mineral. Mag.* **1986**, *50*, 223–229. [CrossRef]
45. Luque, F.J.; Pasteris, J.D.; Wopenka, B.; Rodas, M.; Barrenechea, J.F. Natural fluid-deposited graphite; mineralogical characteristics and mechanisms of formation. *Am. J. Sci.* **1998**, *298*, 471–498. [CrossRef]
46. Deines, P. The isotopic composition of reduced organic carbon. In *The Terrestrial Environment, A*; Fritz, P., Fontes, J.C., Eds.; Elsevier: London, UK, 1980; Volume 1, pp. 329–406. [CrossRef]
47. Valley, J.W. Stable isotope geochemistry of metamorphic rocks. *Rev. Mineral. Geochem.* **1986**, *16*, 445–489. [CrossRef]
48. Hoefs, J. Variations of stable isotope ratios in nature. In *Stable Isotope Geochemistry*; Springer: Berlin/Heidelberg, Germany, 2009; pp. 93–227. [CrossRef]
49. Feybesse, J.L.; Billa, M.; Guerrot, C.; Duguey, E.; Lescuyer, J.-L.; Milesi, J.-P.; Bouchot, V. The Paleoproterozoic Ghanaian province: Geodynamic model and ore controls, including regional stress modeling. *Precambrian Res.* **2006**, *149*, 149–196. [CrossRef]
50. Block, S.; Ganne, J.; Baratoux, L.; Zeh, A.; Parra-Avila, L.A.; Jessell, M.; Ailleres, L.; Siebenaller, L. Petrological and geochronological constraints on lower crust exhumation during Paleoproterozoic (Eburnean) orogeny, NW Ghana, West African Craton. *J. Metamorph. Geol.* **2015**, *33*, 463–494. [CrossRef]
51. Satish-Kumar, M. Carbon isotopic composition of graphite in metamorphic rocks from Lützow-Holm Complex, East Antarctica: Implications for carbon geodynamic cycle in continental crust. *J. Mineral. Petrol. Sci.* **2023**, *118*, 230401. [CrossRef]
52. Cullers, R.L. The geochemistry of shales, siltstones and sandstones of Pennsylvanian–Permian age, Colorado, USA: Implications for provenance and metamorphic studies. *Lithos* **2000**, *51*, 181–203. [CrossRef]

53. Condie, K.C. *Earth as an Evolving Planetary System*, 3rd ed.; Elsevier: London, UK, 2015; Available online: https://books.google.co.in/books?hl=en&lr=&id=2Ss_EAAAQBAJ (accessed on 19 September 2026).
54. Pearce, J.A. Geochemical fingerprinting of oceanic basalts with applications to ophiolite classification and the search for Archean oceanic crust. *Lithos* **2008**, *100*, 14–48. [CrossRef]
55. Cabanis, B. Le diagramme La/10–Y/15–Nb/8: Un outil pour la discrimination des series volcaniques et la mise en evidence des processus de melange et/ou de contamination crustale. *Comptes Rendus l'Acad. Sci. Sér. II* **1989**, *309*, 2023–2029.
56. Pearce, J.A.; Harris, N.B.W.; Tindle, A.G. Trace element discrimination diagrams for the tectonic interpretation of granitic rocks. *J. Petrol.* **1984**, *25*, 956–983. [CrossRef]
57. Eby, G.N. Chemical subdivision of the A-type granitoids: Petrogenetic and tectonic implications. *Geology* **1992**, *20*, 641–644. [CrossRef]
58. Whalen, J.B.; Currie, K.L.; Chappell, B.W. A-type granites: Geochemical characteristics, discrimination and petrogenesis. *Contrib. Mineral. Petrol.* **1987**, *95*, 407–419. [CrossRef]
59. Ohmoto, H.; Goldhaber, M.B. Sulfur and carbon isotopes. In *Geochemistry of Hydrothermal Ore Deposits*, 3rd ed.; Barnes, H.L., Ed.; John Wiley & Sons: Hoboken, NJ, USA, 1997; pp. 517–611.
60. Deines, P. The carbon isotope geochemistry of mantle xenoliths. *Earth-Sci. Rev.* **2002**, *58*, 247–278. [CrossRef]

Disclaimer/Publisher's Note: The statements, opinions and data contained in all publications are solely those of the individual author(s) and contributor(s) and not of MDPI and/or the editor(s). MDPI and/or the editor(s) disclaim responsibility for any injury to people or property resulting from any ideas, methods, instructions or products referred to in the content.